SECOND-ORDER CYCLOSTATIONARITY OF CP-SCLD SIGNALS: THEORETICAL DEVELOPMENTS AND APPLICATIONS TO JOINT SIGNAL DETECTION AND CLASSIFICATION AND BLIND PARAMETER ESTIMATION

QIYUN ZHANG

Second-Order Cyclostationarity of CP-SCLD Signals: Theoretical Developments and Applications to Joint Signal Detection and Classification and Blind Parameter Estimation

by

© Qiyun Zhang

A thesis submitted to the School of Graduate Studies

in partial fulfilment of the requirements for the degree of

Master of Engineering

Faculty of Engineering and Applied Science

Memorial University of Newfoundland

September 2010

St. John's Newfoundland

Abstract

Orthogonal frequency division multiplexing (OFDM) has been adopted in a number of applications in recent years, due to the advantage of resistance to frequency selective fading with a simply equalization. Cyclically prefixed single carrier (CP-SC) modulation has been introduced as an alternative technology with similar performance while avoiding the peak-to-average power problem of the OFDM. As such, joint detection and classification and blind parameter estimation of OFDM and CP-SC signals become a key task in applications such as spectrum awareness in cognitive radio, spectrum monitoring and surveillance, and signal intelligence.

OFDM signal detection and classification, and parameter estimation have been intensively investigated lately. Many of the proposed methods for detection, classification, and parameter estimation of OFDM signals are cyclostationarity-based. To the best of our knowledge there is not such work for CP-SC modulation. In this thesis, the second-order cyclostationarity of CP-single carrier linearly digitally modulated (CP-SCLD) signals is studied, and analytical closed-form expressions are derived for the cyclic autocorrelation function (CAF), set of cycle frequencies (CFs), spectral correlation density function (SCD), as well as the condition to avoid aliasing in cycle and spectral frequency domain of such signal are derived. Based on these findings, we propose algorithms to discriminate between CP-SCLD, OFDM, SCLD, and noise, and to blindly estimate the CP-SCLD block transmission parameters. Simulation and experimental results show the efficiency of the proposed algorithms under low SNRs, short sensing times, and diverse channel conditions. The algorithms have the advantage of avoiding requirements for the recovery of carrier, waveform, and symbol timing information, and the estimation of signal and noise powers.

Acknowledgements

I am heartily grateful to my supervisor, Dr. Octavia Dobre, from Memorial University of Newfoundland, for her suggestions and encouragements helped me throughout my master's program.

I would like to acknowledge the generous financial support from the Defence Research and Development Canada, Ottawa, and be a research assistant under contract with DRDC and Memorial University of Newfoundland.

I would also like to acknowledge the support of D-TA Systems Inc. and MITACS for the eight-month internship.

I would also like to thank the students in the Computer Engineering Research Laboratory (CERL) at Memorial University of Newfoundland, for the pleasant working environment.

I would like to express gratitude to my sister and my girlfriend for their encouragements and love.

Lastly, and most important, I am grateful to my parents. They borne, raised, and supported me with endless love. This thesis is dedicated to them.

Contents

List of Figures

List of Tables

List of Abbreviations

AWGN	Additive white Gaussian noise
CAF	Cyclic autocorrelation function
CC	Cyclic cumulant
CF	Cyclic frequency
CM	Cyclic moment
CP	Cyclic prefix
CP-SC	Cyclically prefixed single carrier modulation
CP-SCLD	Cyclically prefixed single carrier linearly digitally modulated signal
i.i.d.	independent and identically distributed
LTE	Long term evolution
NMSE	Normalized mean square error
OFDM	Orthogonal frequency division multiplexing
PSK	Phase shift keying
QAM	Quadrature amplitude modulation
SCD	Spectral correlation density function
SCLD	Single carrier linear digital modulations
SNR	Signal-to-noise ratio
VSA	Vector signal analyzer
VSG	Vector signal generator
WiMAX	Worldwide interoperability for microwave access
WLAN	Wireless local area network

WMAN	Wireless metropolitan network
w.r.t.	with respect to

List of Symbols

a	Amplitude factor
b	Block index of the CP-SCLD signal
$\bar{c}_r(t;\bar{\tau})_{2,1}$	Second-order (one-conjugate) time-varying cumulant at time t and delay $\bar{\tau}$
$\bar{c}_r(\bar{\beta};\bar{\tau})_{2,1}$	Second-order (one-conjugate) cyclic cumulant at CF $\bar{\beta}$ and delay $\bar{\tau}$
	or cyclic autocorrelation function at CF $\bar{\beta}$ and delay $\bar{\tau}$
$c_{s,2,1}$	Second-order (one-conjugate) cumulant for the signal constellation
$c_w(\beta;\tau)_{2,1}$	The cyclic autocorrelation function of $w(n)$ at CF β and delay τ
$\bar{C}_r(\bar{\beta};\bar{f})_{2,1}$	The spectral correlation density function at CF $\bar{\beta}$ and spectral frequency $\bar{f}$
$\mathrm{Cum}[\cdot]$	Cumulant operator
D	The number of samples over an OFDM symbol
$\delta(t)$	The Dirac delta function
Δf_c	Frequency offset
Δf_K	Frequency separation between two adjacent subcarriers
$\mathrm{E}[\cdot]$	Statistical expectation
ε	Timing offset
f_s	Sampling rate
$f_{2,1}(l;\tau)$	Second-order (one-conjugate) lag product used in the cyclostationarity test
$g(t)$	Overall impulse response of the transmit and receive filters
$G(f)$	The Fourier transform of $g(t)$
Γ	Threshold value used in the cyclostationarity test
$h(t)$	The impulse response of the time dispersive channel

$H(f)$	The Fourier transform of $h(t)$
$\mathrm{Im}\{\cdot\}$	The imaginary part
K	The number of subcarriers of OFDM signal
$\tilde{\kappa}_{2,1,c}$	Set of the second-order CFs (for cumulants)
$\tilde{\kappa}_{2,1,m}$	Set of the second-order CFs (for moments)
l	Symbol index within a CP-SCLD block
L	The number of cyclic prefix symbols in a CP-SCLD block
$\tilde{m}_r(t;\bar{\tau})_{2,1}$	Second-order (one-conjugate) time-varying moment at time t and delay $\bar{\tau}$
$\tilde{m}_r(\tilde{\alpha};\bar{\tau})_{2,1}$	Second-order (one-conjugate) cyclic moment at CF $\tilde{\alpha}$ and delay $\bar{\tau}$
N	The number of information data symbols in a CP-SCLD block
$P_{cr}^{(i\|i)}$	The probabilities of correct signal recognition
$\Psi_{2,1}$	The test statistic used in the cyclostationarity test
r	Roll-off factor
$r(n)$	Discrete-time received signal
$r(t)$	Continuous-time received signal
$\mathrm{Re}\{\cdot\}$	The real part
ρ	Oversampling factor
$s_{b,l}$	Symbol transmitted within the l-th symbol period of CP-SCLD block b
$s_{k,l}$	Symbol transmitted on the k-th subcarrier over the l-th OFDM symbol period
$\Sigma_{2,1}$	Covariance matrix used in the cyclostationarity test
T	Symbol period
T_{cp}	The CP duration of OFDM signal
T_u	The useful symbol duration of OFDM signal

θ	Phase offset
$w(n)$	Discrete-time complex Gaussian noise with zero mean
$w(t)$	Complex Gaussian noise with zero mean
W	Single-side band of $g(t)$
$\otimes$	Convolution operator
$*$	Conjugation operator
$\Im\{\cdot\}$	The Fourier transform
$\lfloor\cdot\rceil$	The nearest integer function

Chapter 1

Introduction

Over the past decade, orthogonal frequency-division multiplexing (OFDM) has become a widely used modulation technique in a number of applications, including broadband wireless local and metropolitan area networks (WLAN and WMAN) [1, 2]. OFDM has been proposed as a solution to combat the effect of multipath fading, in which equalization is drastically simplified [3]. Cyclically prefixed single carrier (CP-SC) modulation has been introduced as an alternative, which provides similar performance, efficiency, and low signal processing advantages of OFDM [4–6]. In addition, unlike OFDM, CP-SC does not suffer from the peak-to-average power and carrier synchronization problems [5, 6]. CP-SC has been adopted in the specifications of the WMAN standard IEEE 802.16 [2] and Long term evolution (LTE) systems [7, 8]. The comparison between OFDM and CP-SC under diverse scenario has been an intensive topic of research for the last two decades [4–6]. When compared with the previous work related to CP-SC modulation, this work investigates the second-order cyclostationarity of such signals, and explores it for joint signal detection and classification.

Blind signal recognition, which encompasses both modulation classification and parameter estimation, is a key task in a variety of military and commercial applications, such as electronic warfare, surveillance control of broadcasting activities, and spectrum awareness in cognitive radio systems [9–11]. Recently, OFDM signal detection and classification has been intensively researched in the context of cognitive radio [12–19]. Many of the proposed methods for detection and classification of OFDM signals are cyclostationarity-based [13–19], with some of them employing the detection of the CP-induced peaks in the cyclic autocorrelation function (CAF) [13–16]. Other methods involve the detection of cyclostationary signatures that are artificially created and intentionally embedded in the OFDM signals for detection and classification purposes [17,18]. In these methods, message symbols are redundantly transmitted on more than one subcarrier, such that a correlation pattern is created and a cyclostationary feature is embedded in the signal. Subcarrier set mapping permits cyclostationary signatures to be embedded in data-carrying waveforms without adding significant complexity to existing transmitter designs. By using this approach, signals may be uniquely classified by the cyclic frequency (CF) created by the embedded signature. The problem in this case is that signature embedding comes at the price of additional overhead and reduction in the data rate. The reduction in the data rate is caused by wasting some subcarriers for signature embedding, while these can otherwise be used for data transmission. The cyclostationarity induced by pilot symbols is explored in [19]; however, it is assumed that the pattern of the pilots is known at the receive-side.

Although modulation classification and parameter estimation of OFDM and SC signals have been extensively studied [9, 12–19], to the best of our knowledge there is not such work carried out for CP-SC modulation. Here we study the second-order cyclostationarity of CP-single carrier linearly digitally modulated signals (CP-SCLD). The analytical expressions for the CAF, set of cycle frequencies (CFs), spectral correlation density function (SCD), as well as the condition to avoid aliasing in cycle and spectral frequency domains are obtained. Then, we employ such findings to discriminate between CP-SCLD, OFDM, SCLD, and noise, as well as to estimate the CP-SCLD block transmission parameters. Simulations and experiments were carried out, and results reported for joint signal detection, classification, and parameter estimation.

1.1 Thesis Organization

The rest of the thesis is organized as follows.

- Chapter 2 presents the channel and signal models; a mathematical model is introduced for the CP-SCLD signals.
- Chapter 3 presents the new findings on the second-order CP-SCLD signal cyclostationarity, as well as the condition to avoid aliasing.
- In Chapter 4 we describe a proposed signal detection and classification algorithm. In addition, performance of this algorithm is investigated by both simulations and experiments.
- In Chapter 5 we propose an algorithm for blind parameter estimation of CP-SCLD block transmission. The performance results obtained through simulation and experiments are also presented.
- Chapter 6 provides conclusions and suggestions for future work.

1.2 Major Contributions of the Thesis

Major contributions presented in each chapter are:

- Chapter 2: Signal model for the CP-SCLD signals.
- Chapter 3: The CAF, CF, and SCD analytical expressions for the CP-SCLD signal and the condition on the oversampling factor to eliminate aliasing in both cycle and spectral frequency domains.
- Chapter 4: Proposed algorithm for joint signal detection and classification, with simulation and experimental results.
- Chapter 5: Proposed algorithm for blind parameter estimation of CP-SCLD signals, with simulation and experimental results.

Some of these contributions were published, as follows:

- A. Punchihewa, Q. Zhang, O. A. Dobre, C. Spooner, S. Rajan, and R. Inkol, "On the nth-order cyclostationarity of OFDM signals in time dispersive channels: theoretical developments and applications," *IEEE Transactions of Wireless Communications*, March 2009, vol. 9, pp. 2588-2599.
- Q. Zhang, O. A. Dobre, S. Rajan, and R. Inkol, "Cyclostationarity approach to joint blind estimation of CP-SCLD block transmission parameters for cognitive radio," in *Proc. IEEE DySPAN*, 2010, pp. 1-5.
- Q. Zhang, O. A. Dobre, S. Rajan, and R. Inkol, "Cyclostationarity approach for the recognition of cyclically prefixed single carrier signals in cognitive radio," in *Proc. IEEE ICC*, 2010, pp. 1-6.

- Q. Zhang, O. A. Dobre, S. Rajan, and R. Inkol, "On the second-order cyclostationarity for joint signal detection and classification in cognitive radio systems," in *Proc. CCECE* 2009, St. John's, Canada, pp. 204-208 (Invited Paper).

- Q. Zhang, O. A. Dobre, S. Rajan, and R. Inkol, "On the Application of Second-Order Cyclostationarity to Signal Recognition," in *Proc. IEEE NECEC*, 2008, St. John's, Canada. Wally Read Best GOLD Paper Award.

- A. Punchihewa, O. A. Dobre, Q. Zhang, S. Rajan, and R. Inkol, "The Nth-Order Cyclostationarity of OFDM Signals in Time Dispersive Channels," in *Proc. ASILOMAR*, 2008, Pacific Grove, CA, USA, pp. 574-580.

- O. A. Dobre, Q. Zhang, S. Rajan, and R. Inkol, "Second-Order Cyclostationarity of Cyclically Prefixed Single Carrier Linear Digital Modulations with Applications to Signal Recognition," in *Proc. IEEE GLOBECOM*, 2008, New Orleans, USA, pp. 1-5.

Chapter 2

Channel and Signal Models

The signals of interest are CP-SCLD, SCLD, and OFDM. In this chapter we mathematically formulate the model for the CP-SCLD signals, which are adopted in the worldwide interoperability for microwave access (WiMAX) and LTE standards for the uplink communication. We also provide the time dispersive channel model, as well as the SCLD and OFDM signal models.

2.1 Channel Model

The signals of interest are transmitted through a time dispersive channel, which also corrupts the signal by adding white Gaussian noise. The impulse response of the time dispersive channel is [20]

$$h(t) = \sum_{m=1}^{M} h(\xi_m)\delta(t - \xi_m), \tag{2.1}$$

where $h(\xi_m)$ is the channel coefficient at delay ξ_m, $m = 1, \ldots, M$, and $\delta(t)$ is the Dirac delta function.

2.2 CP-SCLD Signal Model

The received baseband signals are considered to be affected by the time dispersion introduced by the channel, additive Gaussian noise, and phase, frequency and timing offsets. A block transmission scheme is used in the CP-SCLD based systems, with a block consisting of a cyclic prefix (CP) of L symbols added at the beginning of every N information data symbols [4, 5]. The CP is formed by repeating the last L symbols from the N information data symbols ($L < N$) of the block. Fig. 2.1 shows the structure of a CP-SCLD transmission block. Hence, we express the CP-SCLD signal as

$$
\begin{aligned}
r_{\text{CP-SCLD}}(t) = a e^{j\theta} e^{j2\pi\Delta f_c t} \sum_{b=-\infty}^{\infty} \sum_{l=0}^{N+L-1} \sum_{m=1}^{M} s_{b,l} h(\xi_m) \\
\times g(t - \xi_m - b(N+L)T - lT - \varepsilon T) + w(t),
\end{aligned}
\tag{2.2}
$$

where a is the amplitude, θ is the phase, Δf_c is the frequency offset, T is the symbol period, ε $(0 \leq \varepsilon < 1)$ is the timing offset, b is the block index, l is the symbol index within a block, and $s_{b,l}$ is the symbol transmitted within the l-th symbol period of block b, $g(t)$ is the overall impulse response of the transmit and receive filters, given by $g(t) = g^{tr}(t) \otimes g^{rec}(t)$, with $g^{tr}(t)$ and $g^{rec}(t)$ as the impulse response of the transmit and receive filters, respectively, and $\otimes$ as convolution, and $w(t)$ is the complex Gaussian noise with zero mean.

Figure 2.1: CP-SCLD transmission block structure.

A discrete-time baseband signal, $r_{\text{CP-SCLD}}(n)$, is obtained by oversampling $r_{\text{CP-SCLD}}(t)$

at a sampling frequency $f_s = \frac{\rho}{T}$, with ρ as the oversampling factor,

$$r_{\text{CP-SCLD}}(n) = a e^{j\theta} e^{j\frac{2\pi}{\rho}\Delta f_c T n} \sum_{b=-\infty}^{\infty} \sum_{l=0}^{N+L-1} \sum_{m=1}^{M} s_{b,l} h(\zeta_m) \times g(n - \zeta_m - b(N+L)\rho - l\rho - \varepsilon\rho) + w(n), \quad (2.3)$$

where $w(n)$ is the discrete-time zero-mean complex Gaussian noise and $\zeta_m = \bar{\zeta}_m f_s$ (not necessarily an integer).

2.3 SCLD and OFDM Signal Models

The continuous-time baseband equivalent of the received SCLD signals is given by [13]

$$r_{\text{SCLD}}(t) = a e^{j\theta} e^{j2\pi\Delta f_c t} \sum_{l=-\infty}^{\infty} \sum_{m=1}^{M} s_l h(\bar{\zeta}_m) g(t - \bar{\zeta}_m - lT - \varepsilon T) + w(t), \quad (2.4)$$

where s_l is the symbol transmitted in the l-th symbol period.

Similar to the CP-SCLD signal, the discrete-time baseband SCLD signal, $r_{\text{SCLD}}(n)$, is given as

$$r_{\text{SCLD}}(n) = a e^{j\theta} e^{j\frac{2\pi}{\rho}\Delta f_c T n} \sum_{l=-\infty}^{\infty} \sum_{m=1}^{M} s_l h(\zeta_m) g(n - \zeta_m - l\rho - \varepsilon\rho) + w(n). \quad (2.5)$$

The received continuous-time baseband equivalent OFDM signal is given by [13]

$$r_{\text{OFDM}}(t) = a e^{j\theta} e^{j2\pi\Delta f_c t} \sum_{k=0}^{K-1} \sum_{l=-\infty}^{\infty} \sum_{m=1}^{M} s_{k,l} h(\bar{\zeta}_m) e^{j2\pi k \Delta f_K (t - \bar{\zeta}_m - lT - \varepsilon T)} \times g(t - \bar{\zeta}_m - lT - \varepsilon T) + w(t), \quad (2.6)$$

where K is the number of subcarriers, $s_{k,l}$ is the symbol transmitted on the k-th subcarrier over the l-th OFDM symbol period, Δf_K is the frequency separation between two adjacent subcarriers, and T is the OFDM symbol period. $T = T_u + T_{\text{cp}}$, where $T_u = \frac{1}{\Delta f_K}$ is the useful symbol duration and T_{cp} is the CP duration.

The discrete-time baseband OFDM signal, $r_{\text{OFDM}}(n)$, is obtained by oversampling $r_{\text{OFDM}}(t)$ at a sampling frequency $f_s = \rho K T_u{}^{-1}$, with ρ as the oversampling factor per subcarrier. Note that for SCLD and CP-SCLD $K = 1$ and ρ simply becomes the oversampling factor. The discrete-time baseband equivalent lowpass OFDM received signal can be expressed as

$$\begin{aligned} r_{\text{OFDM}}(n) = {} & a e^{j\theta} e^{j\frac{2\pi}{\rho K}\Delta f_c T_u n} \sum_{k=0}^{K-1} \sum_{l=-\infty}^{\infty} \sum_{m=1}^{M} s_{k,l}\, h(\zeta_m)\, e^{j\frac{2\pi}{\rho K} k(n-\zeta_m - lD - \varepsilon D)} \\ & \times g(n - \zeta_m - lD - \varepsilon D) + w(n), \end{aligned} \tag{2.7}$$

where $D = \rho K(1 + T_{\text{cp}} T_u^{-1})$ is the number of samples over an OFDM symbol.

Regardless of the signal type, the symbols correspond either to a quadrature amplitude modulation (QAM) or phase shift keying (PSK) signal constellation, and are assumed to be independent and identically distributed (i.i.d.) random variables.

We should note that for the signal recognition, the signals of interest are assumed to have the same bandwidth.

2.4 Summary

In this chapter we mathematically modeled the CP-SCLD signals. We also provided the expression for the continuous-time and discrete-time baseband SCLD and OFDM signal models. All the signals of interest are considered to be affected by the time dispersive channel, additive Gaussian noise, and phase, frequency and timing offsets.

Chapter 3

Second-Order Cyclostationarity of Signals of Interest

In this chapter we provide new findings related to the second-order cyclostationarity of CP-SCLD signals. The analytical expressions for the CAF, CF, and SCD are provided, as well as the condition on the oversampling factor to eliminate aliasing in both cycle and spectral frequency domains. In addition, we present the second-order cyclostationarity in terms of CAF for the SCLD and OFDM signals. The second-order cyclostationarity of these signals will be further exploited in Chapter 4 and Chapter 5, where we propose a joint detection and classification algorithm for SCLD, CP-SCLD, and OFDM signals, and a blind parameter estimation algorithm for CP-SCLD signals, respectively. This chapter is organized as follows: -First we introduce the second-order signal cyclostationarity; -Then we study the second-order cyclostationarity of CP-SCLD signals, and present the results for the second-order cyclostationarity of SCLD and OFDM signals.

3.1 Second-Order Cyclostationarity: Definitions

A signal exhibits second-order cyclostationarity if its second- and first-order time-variant cumulants are almost periodic functions of time [21, 22]. For a complex-valued continuous-time second-order cyclostationary process, $r(t)$, the second-order (one-conjugate) time-varying cumulant, $\bar{c}_r(t;\bar{\tau})_{2,1} = \mathrm{Cum}[r(t), r^*(t+\bar{\tau})]$, is an (almost) periodic function of time. Here $\mathrm{Cum}[\cdot]$ represents the cumulant operator, and $\bar{\tau} = [0 \quad \tilde{\tau}]^{\mathsf{T}}$ is the delay vector, with T as the transpose. For simplicity of notation, henceforth we use $\bar{c}_r(t;\tilde{\tau})_{2,1}$ instead of $\bar{c}_r(t;\bar{\tau})_{2,1}$. Also, we refer only to the delay $\tilde{\tau}$ instead of the delay vector $[0 \quad \tilde{\tau}]^{\mathsf{T}}$ when defining second-order statistics. This time-varying cumulant can be expressed as a Fourier series [21,22]

$$\bar{c}_r(t,\tilde{\tau})_{2,1} = \sum_{\tilde{\beta}\in\tilde{\kappa}_{2,1,c}} \bar{c}_r(\tilde{\beta};\tilde{\tau})_{2,1} e^{j2\pi\tilde{\beta}t}, \tag{3.1}$$

where $\tilde{\kappa}_{2,1,c} = \{\tilde{\beta} |\ \bar{c}_r(\tilde{\beta};\tilde{\tau})_{2,1} \neq 0\}$ represents the set of the second-order CFs (for cumulants) and the coefficient $\bar{c}_r(\tilde{\beta};\tilde{\tau})_{2,1}$ is the second-order (one-conjugate) cyclic cumulant (CC) at CF $\tilde{\beta}$ and delay $\tilde{\tau}$, which can be expressed as [21,22]

$$\bar{c}_r(\tilde{\beta};\tilde{\tau})_{2,1} = \lim_{I\to\infty} I^{-1} \int_{-I/2}^{I/2} \bar{c}_r(t;\tilde{\tau})_{2,1} e^{-j2\pi\tilde{\beta}t}\,dt. \tag{3.2}$$

For the second-order cyclostationary process, $r(t)$, the second-order (one-conjugate) time-varying moment function, $\bar{m}_r(t;\tilde{\tau})_{2,1} = \mathrm{E}[r(t)r^*(t+\tilde{\tau})]$, is also an (almost) periodic function of time [21, 22]. Here $\mathrm{E}[\cdot]$ denotes the statistical expectation. This time-varying moment can be also expressed as a Fourier series [21,22]

$$\bar{m}_r(t,\tilde{\tau})_{2,1} = \sum_{\tilde{\alpha}\in\tilde{\kappa}_{2,1,m}} \bar{m}_r(\tilde{\alpha};\tilde{\tau})_{2,1} e^{j2\pi\tilde{\alpha}t}, \tag{3.3}$$

where $\tilde{\kappa}_{2,1,m} = \{\tilde{\alpha} |\ \bar{m}_r(\tilde{\alpha};\tilde{\tau})_{2,1} \neq 0\}$ represents the set of the second-order CFs (for moments), and the coefficient $\bar{m}_r(\tilde{\alpha};\tilde{\tau})_{2,1}$ is the second-order (one-conjugate) cyclic moment

(CM) at CF $\tilde{\alpha}$ and delay $\tilde{\tau}$, given by [21,22]

$$\tilde{m}_r(\tilde{\alpha};\tilde{\tau})_{2,1} = \lim_{I\to\infty} I^{-1} \int_{-I/2}^{I/2} \tilde{m}_r(t;\tilde{\tau})_{2,1} e^{-j2\pi\tilde{\alpha}t} dt. \tag{3.4}$$

The second-order (one-conjugate) time-varying cumulant can be expressed in terms of the second- and first-order moments by using the moment-to-cumulant formula [21,22]

$$\tilde{c}_r(t;\tilde{\tau})_{2,1} = \tilde{m}_r(t;\tilde{\tau})_{2,1} - \tilde{m}_r(t;0)_{1,0}\tilde{m}_r(t;\tilde{\tau})_{1,1}, \tag{3.5}$$

where $\tilde{m}_r(t;0)_{1,0}$ and $\tilde{m}_r(t;\tilde{\tau})_{1,1}$ represent the first-order (zero-conjugate) time-varying moment at zero delay and first-order (one-conjugate) time-varying moment at delay $\tilde{\tau}$, respectively.

By combining (3.1), (3.3) and (3.5), the second-order (one-conjugate) CC at CF $\tilde{\beta}$ and delay $\tilde{\tau}$ can be expressed using the second- and first-order CMs as [21,22]

$$\tilde{c}_r(\tilde{\beta};\tilde{\tau})_{2,1} = \tilde{m}_r(\tilde{\beta};\tilde{\tau})_{2,1} - \sum_{\{\tilde{\alpha}_1,\tilde{\alpha}_2\in\tilde{\kappa}_{2,1,m} | \tilde{\alpha}_1+\tilde{\alpha}_2=\tilde{\beta}\}} \tilde{m}_r(\tilde{\alpha}_1;0)_{1,0}\tilde{m}_r(\tilde{\alpha}_2;\tilde{\tau})_{1,1}, \tag{3.6}$$

where $\tilde{m}_r(\tilde{\alpha}_1;0)_{1,0}$ is the first-order (zero-conjugate) CM of $r(t)$ at CF $\tilde{\alpha}_1$ and zero delay and $\tilde{m}_r(\tilde{\alpha}_2;\tilde{\tau})_{1,1}$ is the first-order (one-conjugate) CM of $r(t)$ at CF $\tilde{\alpha}_2$ and delay $\tilde{\tau}$. Equation (3.6) is referred to as the cyclic moment-to-cumulant formula [21,22].

The SCD of the cyclostationary process, $r(t)$, at CF $\tilde{\beta}$ and spectral frequency $\tilde{f}$, is defined as the Fourier transform of the second-order (one-conjugate) CC [21,23]

$$\tilde{C}_r(\tilde{\beta};\tilde{f})_{2,1} = \int_{-\infty}^{\infty} \tilde{c}_r(\tilde{\beta};\tilde{\tau})_{2,1} e^{-j2\pi\tilde{f}\tilde{\tau}} d\tilde{\tau}. \tag{3.7}$$

A discrete-time signal $r(n) = r(t)|_{t=nf_s^{-1}}$ is obtained by periodically sampling the continuous-time signal $r(t)$ at rate f_s. The SCD of the discrete-time signal, $r(n)$, at CF β and spectral frequency f, is given by [24]

$$C_r(\beta;f)_{2,1} = f_s \sum_{v_1\in Z} \sum_{v_2\in Z} \tilde{C}_r(\tilde{\beta} - v_1 f_s;\tilde{f} - v_2 f_s)_{2,1}, \tag{3.8}$$

where $\beta = \tilde{\beta} f_s^{-1}$, $f = \tilde{f} f_s^{-1}$, Z is the set of all integers, and $v_i, i = 1, 2$, is an integer. One can notice that the SCD of the sampled signal consists of periodic extensions of the SCD of the original continuous-time signal, in both spectral $(\tilde{f} - v_2 f_s)$ and cycle frequency $(\tilde{\beta} - v_1 f_s)$ domains. Two kinds of aliasing effects can appear due to sampling, i.e., spectral aliasing, which is the overlapping of the SCD images with the same CF, and cycle aliasing, which is the overlapping of the SCD images with different CFs. Sampling has to be carried out such that both spectral and cycle aliasing are eliminated. Apparently, for a band-limited signal, the Nyquist condition has to be fulfilled to eliminate aliasing in the spectral frequency domain. For the cycle frequency domain, the support of β has to be found in order to obtain a condition to eliminate cycle aliasing.

Under the assumption of no aliasing, the second-order (one-conjugate) CC, the SCD, and the corresponding set of CFs for the discrete-time signal, $r(n)$, are respectively given by [24]

$$c_r(\beta;\tau)_{2,1} = \tilde{c}_r(\beta f_s; \tau f_s^{-1})_{2,1}, \tag{3.9}$$

$$C_r(\beta;f)_{2,1} = f_s \tilde{C}_r(\beta f_s; f f_s)_{2,1}, \tag{3.10}$$

and

$$\kappa_{2,1,c} = \{\beta \in [-1/2,\ 1/2) \mid \beta = \tilde{\beta} f_s^{-1},\ c_r(\beta;\tau)_{2,1} \neq 0\}, \tag{3.11}$$

where $\tau = \tilde{\tau} f_s$.

Similar expressions can be written for the second-order (one-conjugate) CM of the discrete-time signal, $m_r(\alpha;\tau)_{2,1}$, and the corresponding set of CFs, $\kappa_{2,1,m}$ [24].

The estimator for the second-order (one-conjugate) CM at CF α and delay τ, based on

N_s samples, is given by [25]

$$\hat{m}_r(\alpha;\tau)_{2,1} = \frac{1}{N_s}\sum_{n=0}^{N_s-1} r(n)r^*(n+\tau)e^{-j2\pi\alpha n}. \tag{3.12}$$

Furthermore, the estimator for the second-order (one-conjugate) CC at CF β and delay τ, based on N_s samples, $\hat{c}_r(\beta;\tau)_{2,1}$, can be obtained by applying the cyclic moment-to-cumulant formula given in (3.6), with CMs replaced by their estimates (3.12) [24]. For the estimator of the SCD one can see, for example, [23].

We note that the odd order statistics for the signals of interest, i.e., CP-SCLD, SCLD, and OFDM, equal zero due to the symmetry of the points in the signal constellations. Accordingly, the second-order moments and cumulants, and second-order CM and CC are respectively equal. Henceforth, we will refer to the second-order (one-conjugate) CM and CC as to the CAF.

3.2 Second-Order Cyclostationarity of CP-SCLD Signals

3.2.1 CAF, Set of CFs, and SCD for the CP-SCLD Signals

With the signal model in (2.2), the time-varying second-order (one-conjugate) cumulant of $r_{\text{CP-SCLD}}(t)$ can be expressed as[1]

$$
\begin{aligned}
\tilde{c}_{r_{\text{CP-SCLD}}}(t;\tau)_{2,1} &= \operatorname{Cum}[r_{\text{CP-SCLD}}(t), r^{*}_{\text{CP-SCLD}}(t+\tau)] \\
&= a^{2}e^{-j2\pi\Delta f_c\tau}\sum_{b_1=-\infty}^{\infty}\sum_{b_2=-\infty}^{\infty}\sum_{l_1=0}^{N+L-1}\sum_{l_2=0}^{N+L-1}\operatorname{Cum}[s_{b_1,l_1}, s^{*}_{b_2,l_2}] \\
&\quad\times\sum_{m_1=1}^{M} h(\xi_{m_1})g(t-\xi_{m_1}-b_1(N+L)T-l_1T-\varepsilon T) \\
&\quad\times\sum_{m_2=1}^{M} h^{*}(\xi_{m_2})g^{*}(t-\xi_{m_2}-b_2(N+L)T-l_2T-\varepsilon T+\tau), \quad (3.13)
\end{aligned}
$$

where $*$ denotes conjugation. Based on the cumulant property, according to which the cumulant of two independent random variables equals zero, one can easily notice that the cumulant $\operatorname{Cum}[s_{b_1,l_1}, s^{*}_{b_2,l_2}]$ is zero unless $b_1 = b_2$ (the same data block), and either $l_1 = l_2$ (the same symbol within a block), or $l_2 = l_1 \pm N$ (an information symbol and corresponding symbol in the CP). The former occurs around delays $\xi_{m_2} - \xi_{m_1}$[2], $m_1, m_2 = 1, \ldots, M$, whereas the latter appears around delays $\pm NT + \xi_{m_2} - \xi_{m_1}$[2]. In such cases, $\operatorname{Cum}[s_{b_1,l_1}, s^{*}_{b_2,l_2}]$ equals the second-order (one-conjugate) cumulant for the signal constellation, $c_{s,2,1}$, and (3.13)

[1]Results presented here are for the cumulant of the signal component only; the cumulant of the noise component must be added to the final result.

[2]The delay range depends on the pulse shape.

can be written as

$$
\begin{aligned}
&\tilde{c}_{r_{\text{CP-SCLD}}}(t;\tilde{\tau})_{2,1} = \\
&a^2 e^{-j2\pi\Delta f_c \tilde{\tau}} c_{s,2,1} \sum_{b=-\infty}^{\infty} \sum_{l=0}^{N+L-1} \sum_{m_1=1}^{M} h(\tilde{\zeta}_{m_1}) g(t-\tilde{\zeta}_{m_1} - b(N+L)T - lT - \varepsilon T) \\
&\times \sum_{m_2=1}^{M} h^*(\tilde{\zeta}_{m_2}) g^*(t-\tilde{\zeta}_{m_2} - b(N+L)T - lT - \varepsilon T + \tilde{\tau}) \\
&+ a^2 e^{-j2\pi\Delta f_c \tilde{\tau}} c_{s,2,1} \sum_{b=-\infty}^{\infty} \sum_{l=0}^{L-1} \sum_{m_1=1}^{M} h(\tilde{\zeta}_{m_1}) g(t-\tilde{\zeta}_{m_1} - b(N+L)T - lT - \varepsilon T) \\
&\times \sum_{m_2=1}^{M} h^*(\tilde{\zeta}_{m_2}) g^*(t-\tilde{\zeta}_{m_2} - b(N+L)T - lT + NT - \varepsilon T + \tilde{\tau}) \\
&+ a^2 e^{-j2\pi\Delta f_c \tilde{\tau}} c_{s,2,1} \sum_{b=-\infty}^{\infty} \sum_{l=0}^{L-1} \sum_{m_1=1}^{M} h(\tilde{\zeta}_{m_1}) g(t-\tilde{\zeta}_{m_1} - b(N+L)T - lT - \varepsilon T) \\
&\times \sum_{m_2=1}^{M} h^*(\tilde{\zeta}_{m_2}) g^*(t-\tilde{\zeta}_{m_2} - b(N+L)T - lT - NT - \varepsilon T + \tilde{\tau}),
\end{aligned}
\tag{3.14}
$$

where the first, second, and third terms in the right hand-side hold for delays around $\tilde{\zeta}_{m_2} - \tilde{\zeta}_{m_1}{}^2$, $-NT + \tilde{\zeta}_{m_2} - \tilde{\zeta}_{m_1}{}^2$, and $+NT + \tilde{\zeta}_{m_2} - \tilde{\zeta}_{m_1}{}^2$, respectively. With the notation $k = b(N+L) + l$ used in the first term of the right hand-side of (3.14), and by emphasizing the delay range, this equation can be easily written as

$$
\tilde{c}_{r_{\text{CP-SCLD}}}(t;\tilde{\tau})_{2,1} = \begin{cases}
a^2 e^{-j2\pi\Delta f_c \tilde{\tau}} c_{s,2,1} [\sum_{m_1=1}^{M} h(\tilde{\zeta}_{m_1}) g(t-\tilde{\zeta}_{m_1}) \\
\times \sum_{m_2=1}^{M} h^*(\tilde{\zeta}_{m_2}) g^*(t-\tilde{\zeta}_{m_2}+\tilde{\tau})] \otimes \sum_{k=-\infty}^{\infty} \delta(t-kT-\varepsilon T), \\
\text{for delays around } \tilde{\tau} = \tilde{\zeta}_{m_2} - \tilde{\zeta}_{m_1}{}^2, \\
a^2 e^{-j2\pi\Delta f_c \tilde{\tau}} c_{s,2,1} [\sum_{l=0}^{L-1} \sum_{m_1=1}^{M} h(\tilde{\zeta}_{m_1}) g(t-\tilde{\zeta}_{m_1} - lT) \sum_{m_2=1}^{M} h^*(\tilde{\zeta}_{m_2}) \\
\times g^*(t-\tilde{\zeta}_{m_2} - lT \mp NT + \tilde{\tau})] \otimes \sum_{b=-\infty}^{\infty} \delta(t-b(N+L)T-\varepsilon T), \\
\text{for delays around } \tilde{\tau} = \pm NT + \tilde{\zeta}_{m_2} - \tilde{\zeta}_{m_1}{}^2.
\end{cases}
\tag{3.15}
$$

The Fourier transform of the second-order (one-conjugate) time-varying cumulant of the received baseband CP-SCLD signal with respect to (w.r.t.) t is then given as

$$\Im\{\tilde{c}_{r_{\text{CP-SCLD}}}(t;\tilde{\tau})_{2,1}\} = \begin{cases} a^2 e^{-j2\pi\Delta f_c\tilde{\tau}} c_{s,2,1}\Im\{\sum\limits_{m_1=1}^{M} h(\tilde{\zeta}_{m_1})g(t-\tilde{\zeta}_{m_1}) \\ \times \sum\limits_{m_2=1}^{M} h^*(\tilde{\zeta}_{m_2})g^*(t-\tilde{\zeta}_{m_2}+\tilde{\tau})\} \times \Im\{\sum\limits_{k=-\infty}^{\infty} \delta(t-kT-\varepsilon T)\}, \\ \text{for delays around } \tilde{\tau} = \tilde{\zeta}_{m_2} - \tilde{\zeta}_{m_1}{}^2, \\ a^2 e^{-j2\pi\Delta f_c\tilde{\tau}} c_{s,2,1}\Im\{\sum\limits_{l=0}^{L-1}\sum\limits_{m_1=1}^{M} h(\tilde{\zeta}_{m_1})g(t-\tilde{\zeta}_{m_1}-lT) \sum\limits_{m_2=1}^{M} h^*(\tilde{\zeta}_{m_2}) \\ \times g^*(t-\tilde{\zeta}_{m_2}-lT\mp NT+\tilde{\tau})\} \times \Im\{\sum\limits_{b=-\infty}^{\infty} \delta(t-b(N+L)T-\varepsilon T)\}, \\ \text{for delays around } \tilde{\tau} = \pm NT + \tilde{\zeta}_{m_2} - \tilde{\zeta}_{m_1}{}^2, \end{cases} \tag{3.16}$$

where $\Im\{\cdot\}$ denotes the Fourier transform. By using that the Fourier transform $\Im\{\sum\limits_{k=-\infty}^{\infty} \delta(t-kT)\} = \frac{1}{T}\sum\limits_{k=-\infty}^{\infty} \delta(\tilde{\beta}-\frac{k}{T})$, (3.16) can be easily written as

$$\Im\{\tilde{c}_{r_{\text{CP-SCLD}}}(t;\tilde{\tau})_{2,1}\} = \begin{cases} a^2 e^{-j2\pi\Delta f_c\tilde{\tau}} c_{s,2,1}\frac{1}{T}\int\limits_{-\infty}^{\infty}\sum\limits_{m_1=1}^{M} h(\tilde{\zeta}_{m_1})g(t-\tilde{\zeta}_{m_1}) \sum\limits_{m_2=1}^{M} h^*(\tilde{\zeta}_{m_2}) \\ \times g^*(t-\tilde{\zeta}_{m_2}+\tilde{\tau})e^{-j2\pi\tilde{\beta}t}dt \sum\limits_{k=-\infty}^{\infty} \delta(\tilde{\beta}-\frac{k}{T})e^{-j2\pi\tilde{\beta}\varepsilon T}, \\ \text{for delays around } \tilde{\tau} = \tilde{\zeta}_{m_2} - \tilde{\zeta}_{m_1}{}^2, \\ a^2 e^{-j2\pi\Delta f_c\tilde{\tau}} c_{s,2,1}\frac{1}{(N+L)T}\int\limits_{-\infty}^{\infty}\sum\limits_{l=0}^{L-1}\sum\limits_{m_1=1}^{M} h(\tilde{\zeta}_{m_1})g(t-\tilde{\zeta}_{m_1}-lT) \sum\limits_{m_2=1}^{M} h^*(\tilde{\zeta}_{m_2}) \\ \times g^*(t-\tilde{\zeta}_{m_2}-lT\mp NT+\tilde{\tau})e^{-j2\pi\tilde{\beta}t}dt \sum\limits_{b=-\infty}^{\infty} \delta(\tilde{\beta}-\frac{b}{(N+L)T})e^{-j2\pi\tilde{\beta}\varepsilon T}, \\ \text{for delays around } \tilde{\tau} = \pm NT + \tilde{\zeta}_{m_2} - \tilde{\zeta}_{m_1}{}^2. \end{cases} \tag{3.17}$$

From (3.17) one can easily notice that $\Im\{\tilde{c}_{r_{\text{CP-SCLD}}}(t;\tilde{\tau})_{2,1}\} \neq 0$ only if $\tilde{\beta} = \frac{k}{T}$ or $\tilde{\beta} = \frac{b}{(N+L)T}$, with k and b as integers. By taking the inverse Fourier transform of (3.17), one can further show that $\tilde{c}_{r_{\text{CP-SCLD}}}(t;\bar{\tau})_{2,1}$ can be expressed as

$$
\tilde{c}_{r_{\text{CP-SCLD}}}(t;\bar{\tau})_{2,1} =
\begin{cases}
\sum\limits_{\{\tilde{\beta}\}} \{a^2 e^{-j2\pi\Delta f_c \bar{\tau}} c_{s,2,1} \frac{1}{T} e^{-j2\pi\tilde{\beta}\varepsilon T} \int\limits_{-\infty}^{\infty} \sum\limits_{m_1=1}^{M} h(\tilde{\zeta}_{m_1}) g(t-\tilde{\zeta}_{m_1}) \\
\times \sum\limits_{m_2=1}^{M} h^*(\tilde{\zeta}_{m_2}) g^*(t-\tilde{\zeta}_{m_2}+\bar{\tau}) e^{-j2\pi\tilde{\beta}t} dt\} e^{j2\pi\tilde{\beta}t}, \\
\text{for delays around } \bar{\tau} = \tilde{\zeta}_{m_2} - \tilde{\zeta}_{m_1}{}^2, \text{ and } \tilde{\beta} = \frac{k}{T}, k \text{ integer}, \\
\sum\limits_{\{\tilde{\beta}\}} \{a^2 e^{-j2\pi\Delta f_c \bar{\tau}} c_{s,2,1} \frac{1}{(N+L)T} e^{-j2\pi\tilde{\beta}\varepsilon T} \int\limits_{-\infty}^{\infty} \sum\limits_{l=0}^{L-1} \sum\limits_{m_1=1}^{M} h(\tilde{\zeta}_{m_1}) g(t-\tilde{\zeta}_{m_1}-lT) \\
\times \sum\limits_{m_2=1}^{M} h^*(\tilde{\zeta}_{m_2}) g^*(t-\tilde{\zeta}_{m_2}-lT \mp NT+\bar{\tau}) e^{-j2\pi\tilde{\beta}t} dt\} e^{j2\pi\tilde{\beta}t}, \\
\text{for delays around } \bar{\tau} = \pm NT + \tilde{\zeta}_{m_2} - \tilde{\zeta}_{m_1}{}^2, \text{ and } \tilde{\beta} = \frac{b}{(N+L)T}, b \text{ integer}.
\end{cases}
\tag{3.18}
$$

By using (3.1) and (3.18), one can see that $\{\tilde{\beta}|\tilde{\beta} = \frac{k}{T}, k \text{ integer}\}$ represents the CFs for delays around $\tilde{\zeta}_{m_2} - \tilde{\zeta}_{m_1}{}^2$, whereas $\{\tilde{\beta}|\tilde{\beta} = \frac{b}{(N+L)T}, b \text{ integer}\}$ are the CFs for delays around $\pm NT + \tilde{\zeta}_{m_2} - \tilde{\zeta}_{m_1}{}^2$. As such, the cycle frequency domain is discrete and the spectrum consists of a set of finite-strength additive components. Furthermore, the CAF at corresponding CF $\tilde{\beta}$ can be written as

$$
\tilde{c}_{r_{\text{CP-SCLD}}}(\tilde{\beta};\bar{\tau})_{2,1} =
\begin{cases}
a^2 e^{-j2\pi\Delta f_c \bar{\tau}} c_{s,2,1} \frac{1}{T} e^{-j2\pi\tilde{\beta}\varepsilon T} \int\limits_{-\infty}^{\infty} \sum\limits_{m_1=1}^{M} h(\tilde{\zeta}_{m_1}) g(t-\tilde{\zeta}_{m_1}) \\
\times \sum\limits_{m_2=1}^{M} h^*(\tilde{\zeta}_{m_2}) g^*(t-\tilde{\zeta}_{m_2}+\bar{\tau}) e^{-j2\pi\tilde{\beta}t} dt, \\
\text{for delays around } \bar{\tau} = \tilde{\zeta}_{m_2} - \tilde{\zeta}_{m_1}{}^2, \text{ and } \tilde{\beta} = \frac{k}{T}, k \text{ integer}, \\
a^2 e^{-j2\pi\Delta f_c \bar{\tau}} c_{s,2,1} \frac{1}{(N+L)T} e^{-j2\pi\tilde{\beta}\varepsilon T} \int\limits_{-\infty}^{\infty} \sum\limits_{l=0}^{L-1} \sum\limits_{m_1=1}^{M} h(\tilde{\zeta}_{m_1}) g(t-\tilde{\zeta}_{m_1}-lT) \\
\times \sum\limits_{m_2=1}^{M} h^*(\tilde{\zeta}_{m_2}) g^*(t-\tilde{\zeta}_{m_2}-lT \mp NT+\bar{\tau}) e^{-j2\pi\tilde{\beta}t} dt, \\
\text{for delays around } \bar{\tau} = \pm NT + \tilde{\zeta}_{m_2} - \tilde{\zeta}_{m_1}{}^2, \text{and } \tilde{\beta} = \frac{b}{(N+L)T}, b \text{ integer}.
\end{cases}
\tag{3.19}
$$

By using (3.9), (3.11), and (3.19), it is straightforward to obtain the analytical closed-form expressions for the CAF and set of CFs for the discrete CP-SCLD signals in (2.3) (under the assumption of no aliasing) as

$$
c_{r_{\text{CP-SCLD}}}(\beta;\tau)_{2,1} =
\begin{cases}
a^2 e^{-j\frac{2\pi}{\rho}\Delta f_c T\tau} c_{s,2,1}\frac{1}{\rho} e^{-j2\pi\beta\varepsilon\rho} \sum_{n=-\infty}^{\infty}\sum_{m_1=1}^{M} h(\zeta_{m_1}) g(n-\zeta_{m_1}) \\
\times \sum_{m_2=1}^{M} h^*(\zeta_{m_2}) g^*(n+\tau-\zeta_{m_2}) e^{-j2\pi\beta n} + c_w(\beta;\tau)_{2,1}, \\
\text{for delays around } \tau = \zeta_{m_2} - {\zeta_{m_1}}^2 \text{ and } \beta = \frac{k}{\rho}, k \text{ integer}, \\
a^2 e^{-j\frac{2\pi}{\rho}\Delta f_c T\tau} c_{s,2,1}\frac{1}{(N+L)\rho} e^{-j2\pi\beta\varepsilon\rho} \sum_{l=0}^{L-1}\sum_{n=-\infty}^{\infty}\sum_{m_1=1}^{M} h(\zeta_{m_1}) g(n-\zeta_{m_1}-l\rho) \\
\times \sum_{m_2=1}^{M} h^*(\zeta_{m_2}) g^*(n-\zeta_{m_2}-l\rho \mp N\rho+\tau) e^{-j2\pi\beta n} + c_w(\beta;\tau)_{2,1}, \\
\text{for delays around } \tau = \pm\rho N + \zeta_{m_2} - {\zeta_{m_1}}^2 \text{ and } \beta = \frac{b}{(N+L)\rho}, b \text{ integer},
\end{cases}
\tag{3.20}
$$

and

$$
\begin{aligned}
\kappa_{2,1,c}^{\text{CP-SCLD}} &= \left\{\beta \in [-\frac{1}{2},\frac{1}{2})|\beta = \frac{k}{\rho},\ k \text{ integer, when } \tau \text{ varies around } \zeta_{m_2} - {\zeta_{m_1}}^2\right\} \\
&\cup \left\{\beta \in [-\frac{1}{2},\frac{1}{2})|\beta = \frac{b}{(N+L)\rho},\ b \text{ integer, when } \tau \text{ varies around } \pm\rho N + \zeta_{m_2} - {\zeta_{m_1}}^2\right\},
\end{aligned}
\tag{3.21}
$$

where $c_w(\beta;\tau)$ is the CAF of $w(n)$.

Note that for the CP-SCLD signal, the expression for the CAF in (3.20) is valid only at the CFs given in (3.21) and for delays around $\zeta_{m_2} - {\zeta_{m_1}}^2$ and $\pm\rho N + \zeta_{m_2} - {\zeta_{m_1}}^2$, $m_1, m_2 = 1,\ldots,M$, with the latter due to the existence of the CP in the block transmission. At any other frequencies and delays, the CAF equals zero.

Furthermore, the Fourier transform of the CAF of the received baseband continuous-time CP-SCLD signal w.r.t. $\tilde{\tau}$, which gives the SCD, $\tilde{C}_{r_{\text{CP-SCLD}}}(\tilde{\beta};\tilde{f})_{2,1}$, can be written as the sum of three terms,

$$
\begin{aligned}
&\Im\{\tilde{c}_{r_{\text{CP-SCLD}}}(\tilde{\beta};\bar{\tau})_{2,1}\} = \tilde{C}_{r_{\text{CP-SCLD}}}(\tilde{\beta};\bar{f})_{2,1} \\
&a^2 c_{s,2,1}\tfrac{1}{T}e^{-j2\pi\tilde{\beta}\varepsilon T}\Im\{e^{-j2\pi\Delta f_c\bar{\tau}}\int_{-\infty}^{\infty}\sum_{m_1=1}^{M} h(\tilde{\zeta}_{m_1})g(t-\tilde{\zeta}_{m_1}) \\
&\times \sum_{m_2=1}^{M} h^*(\tilde{\zeta}_{m_2})g^*(t-\tilde{\zeta}_{m_2}+\bar{\tau})e^{-j2\pi\tilde{\beta}t}dt\} \\
&+a^2 c_{s,2,1}\tfrac{1}{(N+L)T}e^{-j2\pi\tilde{\beta}\varepsilon T}\Im\{e^{-j2\pi\Delta f_c\bar{\tau}}\int_{-\infty}^{\infty}\sum_{l=0}^{L-1}\sum_{m_1=1}^{M} h(\tilde{\zeta}_{m_1})g(t-\tilde{\zeta}_{m_1}-lT) \\
&\times \sum_{m_2=1}^{M} h^*(\tilde{\zeta}_{m_2})g^*(t-\tilde{\zeta}_{m_2}-lT+NT+\bar{\tau})e^{-j2\pi\tilde{\beta}t}dt\} \\
&+a^2 c_{s,2,1}\tfrac{1}{(N+L)T}e^{-j2\pi\tilde{\beta}\varepsilon T}\Im\{e^{-j2\pi\Delta f_c\bar{\tau}}\int_{-\infty}^{\infty}\sum_{l=0}^{L-1}\sum_{m_1=1}^{M} h(\tilde{\zeta}_{m_1})g(t-\tilde{\zeta}_{m_1}-lT) \\
&\times \sum_{m_2=1}^{M} h^*(\tilde{\zeta}_{m_2})g^*(t-\tilde{\zeta}_{m_2}-lT-NT+\bar{\tau})e^{-j2\pi\tilde{\beta}t}dt\},
\end{aligned}
\tag{3.22}
$$

where the first term is non-zero at $\tilde{\beta} = \frac{k}{T}$, k integer, and delays around $\bar{\tau} = \tilde{\zeta}_{m_2} - \tilde{\zeta}_{m_1}$, and the second and third terms are non-zero at $\tilde{\beta} = \frac{b}{(N+L)T}$, b integer, and delays around $\bar{\tau} = -NT + \tilde{\zeta}_{m_2} - \tilde{\zeta}_{m_1}$ and $\bar{\tau} = NT + \tilde{\zeta}_{m_2} - \tilde{\zeta}_{m_1}$, respectively.

By emphasizing the discrete CF values, this equation can be rewritten as

$$
\Im\{\tilde{c}_{r_{\text{CP-SCLD}}}(\tilde{\beta};\tilde{\tau})_{2,1}\} = \tilde{C}_{r_{\text{CP-SCLD}}}(\tilde{\beta};\tilde{f})_{2,1}
\begin{cases}
a^2 c_{s,2,1}\frac{1}{T}e^{-j2\pi\tilde{\beta}\varepsilon T}\int\limits_{-\infty}^{\infty} e^{-j2\pi\Delta f_c\tilde{\tau}}\int\limits_{-\infty}^{\infty}\sum\limits_{m_1=1}^{M} h(\tilde{\zeta}_{m_1})g(t-\tilde{\zeta}_{m_1}) \\
\times \sum\limits_{m_2=1}^{M} h^*(\tilde{\zeta}_{m_2})g^*(t-\tilde{\zeta}_{m_2}+\tilde{\tau})e^{-j2\pi\tilde{\beta}t}dt e^{-j2\pi\tilde{f}\tilde{\tau}}d\tilde{\tau} \\
+a^2 c_{s,2,1}\frac{1}{(N+L)T}e^{-j2\pi\tilde{\beta}\varepsilon T}\int\limits_{-\infty}^{\infty} e^{-j2\pi\Delta f_c\tilde{\tau}}\int\limits_{-\infty}^{\infty}\sum\limits_{l=0}^{L-1}\sum\limits_{m_1=1}^{M} h(\tilde{\zeta}_{m_1})g(t-\tilde{\zeta}_{m_1}-lT) \\
\times \sum\limits_{m_2=1}^{M} h^*(\tilde{\zeta}_{m_2})g^*(t-\tilde{\zeta}_{m_2}-lT+NT+\tilde{\tau})e^{-j2\pi\tilde{\beta}t}dt e^{-j2\pi\tilde{f}\tilde{\tau}}d\tilde{\tau} \\
+a^2 c_{s,2,1}\frac{1}{(N+L)T}e^{-j2\pi\tilde{\beta}\varepsilon T}\int\limits_{-\infty}^{\infty} e^{-j2\pi\Delta f_c\tilde{\tau}}\int\limits_{-\infty}^{\infty}\sum\limits_{l=0}^{L-1}\sum\limits_{m_1=1}^{M} h(\tilde{\zeta}_{m_1})g(t-\tilde{\zeta}_{m_1}-lT) \\
\times \sum\limits_{m_2=1}^{M} h^*(\tilde{\zeta}_{m_2})g^*(t-\tilde{\zeta}_{m_2}-lT-NT+\tilde{\tau})e^{-j2\pi\tilde{\beta}t}dt e^{-j2\pi\tilde{f}\tilde{\tau}}d\tilde{\tau}, \\
\text{for CF } \tilde{\beta}=\frac{k}{T}, k \text{ integer}, \\
a^2 c_{s,2,1}\frac{1}{(N+L)T}e^{-j2\pi\tilde{\beta}\varepsilon T}\int\limits_{-\infty}^{\infty} e^{-j2\pi\Delta f_c\tilde{\tau}}\int\limits_{-\infty}^{\infty}\sum\limits_{l=0}^{L-1}\sum\limits_{m_1=1}^{M} h(\tilde{\zeta}_{m_1})g(t-\tilde{\zeta}_{m_1}-lT) \\
\times \sum\limits_{m_2=1}^{M} h^*(\tilde{\zeta}_{m_2})g^*(t-\tilde{\zeta}_{m_2}-lT+NT+\tilde{\tau})e^{-j2\pi\tilde{\beta}t}dt e^{-j2\pi\tilde{f}\tilde{\tau}}d\tilde{\tau} \\
+a^2 c_{s,2,1}\frac{1}{(N+L)T}e^{-j2\pi\tilde{\beta}\varepsilon T}\int\limits_{-\infty}^{\infty} e^{-j2\pi\Delta f_c\tilde{\tau}}\int\limits_{-\infty}^{\infty}\sum\limits_{l=0}^{L-1}\sum\limits_{m_1=1}^{M} h(\tilde{\zeta}_{m_1})g(t-\tilde{\zeta}_{m_1}-lT) \\
\times \sum\limits_{m_2=1}^{M} h^*(\tilde{\zeta}_{m_2})g^*(t-\tilde{\zeta}_{m_2}-lT-NT+\tilde{\tau})e^{-j2\pi\tilde{\beta}t}dt e^{-j2\pi\tilde{f}\tilde{\tau}}d\tilde{\tau}, \\
\text{for CF } \tilde{\beta}=\frac{b}{(N+L)T}, b\neq k(N+L), k, b \text{ integers.}
\end{cases} \tag{3.23}
$$

Note that we have three terms for CF $\tilde{\beta}=\frac{k}{T}$, k integer, with the first for a delay around $\tilde{\zeta}_{m_2}-\tilde{\zeta}_{m_1}$, the second for a delay around $-NT+\tilde{\zeta}_{m_2}-\tilde{\zeta}_{m_1}$, and the third for a delay around $NT+\tilde{\zeta}_{m_2}-\tilde{\zeta}_{m_1}$. The second and third terms are yielded for integer values of b in (3.22) equal to $k(N+L)$, k integer. On the other hand, we have two terms for CF $\tilde{\beta}=\frac{b}{(N+L)T}$, $b\neq k(N+L)$, k, b integers, for delays around $\mp NT+\tilde{\zeta}_{m_2}-\tilde{\zeta}_{m_1}$, respectively.

With the change of variables $v_1=t+\tilde{\tau}$, $v_2=t+NT+\tilde{\tau}$, $v_3=t-NT+\tilde{\tau}$, and by emphasizing the convolution between $g(t)$ and the channel, (3.23) can be expressed as

$$
\begin{aligned}
&\mathfrak{I}\{\tilde{c}_{r_{\text{CP-SCLD}}}(\tilde{\beta};\tilde{\tau})_{2,1}\} = \tilde{C}_{r_{\text{CP-SCLD}}}(\tilde{\beta};\tilde{f})_{2,1} \\
&\begin{cases}
a^2 c_{s,2,1}\frac{1}{T}e^{-j2\pi\tilde{\beta}\varepsilon T}\int\limits_{-\infty}^{\infty}[h(t)\otimes g(t)]e^{-j2\pi(\tilde{\beta}-\tilde{f}-\Delta f_c)t}dt \\
\times\int\limits_{-\infty}^{\infty}[(h(v_1)\otimes g(v_1))e^{-j2\pi(-\tilde{f}-\Delta f_c)v_1}]^* dv_1 \\
+a^2 c_{s,2,1}\frac{1}{(N+L)T}e^{-j2\pi\tilde{\beta}\varepsilon T}e^{-j2\pi(\tilde{f}+\Delta f_c)NT}\sum\limits_{l=0}^{L-1}\int\limits_{-\infty}^{\infty}[h(t)\otimes g(t-lT)]e^{-j2\pi(\tilde{\beta}-\tilde{f}-\Delta f_c)t}dt \\
\times\int\limits_{-\infty}^{\infty}[(h(v_2)\otimes g(v_2-lT))e^{-j2\pi(-\tilde{f}-\Delta f_c)v_2}]^* dv_2 \\
+a^2 c_{s,2,1}\frac{1}{(N+L)T}e^{-j2\pi\tilde{\beta}\varepsilon T}e^{-j2\pi(\tilde{f}+\Delta f_c)(-NT)}\sum\limits_{l=0}^{L-1}\int\limits_{-\infty}^{\infty}[h(t)\otimes g(t-lT)]e^{-j2\pi(\tilde{\beta}-\tilde{f}-\Delta f_c)t}dt \\
\times\int\limits_{-\infty}^{\infty}[(h(v_3)\otimes g(v_3-lT))e^{-j2\pi(-\tilde{f}-\Delta f_c)v_3}]^* dv_3, \\
\text{for CF } \tilde{\beta}=\frac{k}{T}, k \text{ integer}, \\
a^2 c_{s,2,1}\frac{1}{(N+L)T}e^{-j2\pi\tilde{\beta}\varepsilon T}e^{-j2\pi(\tilde{f}+\Delta f_c)NT}\sum\limits_{l=0}^{L-1}\int\limits_{-\infty}^{\infty}[h(t)\otimes g(t-lT)]e^{-j2\pi(\tilde{\beta}-\tilde{f}-\Delta f_c)t}dt \\
\times\int\limits_{-\infty}^{\infty}[(h(v_2)\otimes g(v_2-lT))e^{-j2\pi(-\tilde{f}-\Delta f_c)v_2}]^* dv_2 \\
+a^2 c_{s,2,1}\frac{1}{(N+L)T}e^{-j2\pi\tilde{\beta}\varepsilon T}e^{-j2\pi(\tilde{f}+\Delta f_c)(-NT)}\sum\limits_{l=0}^{L-1}\int\limits_{-\infty}^{\infty}[h(t)\otimes g(t-lT)]e^{-j2\pi(\tilde{\beta}-\tilde{f}-\Delta f_c)t}dt \\
\times\int\limits_{-\infty}^{\infty}[(h(v_3)\otimes g(v_3-lT))e^{-j2\pi(-\tilde{f}-\Delta f_c)v_3}]^* dv_3, \\
\text{for CF } \tilde{\beta}=\frac{b}{(N+L)T}, b\neq k(N+L), k,b \text{ integers}.
\end{cases}
\end{aligned}
\tag{3.24}
$$

Further, by defining $G(f)$ and $H(f)$ as the Fourier transform of $g(t)$ and $h(t)$, respectively, one can express (3.24) as

$$
\begin{aligned}
&\Im\{\tilde{c}_{r_{\text{CP-SCLD}}}(\tilde{\beta};\tilde{\tau})_{2,1}\} = \tilde{C}_{r_{\text{CP-SCLD}}}(\tilde{\beta};\tilde{f})_{2,1} \\
&\begin{cases}
a^2 c_{s,2,1}\frac{1}{T}e^{-j2\pi\tilde{\beta}\varepsilon T}H(\tilde{\beta}-\tilde{f}-\Delta f_c)G(\tilde{\beta}-\tilde{f}-\Delta f_c)H^*(-\tilde{f}-\Delta f_c)G^*(-\tilde{f}-\Delta f_c) \\
+\,a^2 c_{s,2,1}\frac{1}{(N+L)T}e^{-j2\pi\tilde{\beta}\varepsilon T}e^{-j2\pi(\tilde{f}+\Delta f_c)NT}\sum_{l=0}^{L-1}e^{-j2\pi\tilde{\beta}lT} \\
\times H(\tilde{\beta}-\tilde{f}-\Delta f_c)G(\tilde{\beta}-\tilde{f}-\Delta f_c)H^*(-\tilde{f}-\Delta f_c)G^*(-\tilde{f}-\Delta f_c) \\
+\,a^2 c_{s,2,1}\frac{1}{(N+L)T}e^{-j2\pi\tilde{\beta}\varepsilon T}e^{-j2\pi(\tilde{f}+\Delta f_c)(-NT)}\sum_{l=0}^{L-1}e^{-j2\pi\tilde{\beta}lT} \\
\times H(\tilde{\beta}-\tilde{f}-\Delta f_c)G(\tilde{\beta}-\tilde{f}-\Delta f_c)H^*(-\tilde{f}-\Delta f_c)G^*(-\tilde{f}-\Delta f_c), \\
\text{for CF } \tilde{\beta}=\frac{k}{T}, k \text{ integer}, \\
+\,a^2 c_{s,2,1}\frac{1}{(N+L)T}e^{-j2\pi\tilde{\beta}\varepsilon T}e^{-j2\pi(\tilde{f}+\Delta f_c)NT}\sum_{l=0}^{L-1}e^{-j2\pi\tilde{\beta}lT} \\
\times H(\tilde{\beta}-\tilde{f}-\Delta f_c)G(\tilde{\beta}-\tilde{f}-\Delta f_c)H^*(-\tilde{f}-\Delta f_c)G^*(-\tilde{f}-\Delta f_c) \\
+\,a^2 c_{s,2,1}\frac{1}{(N+L)T}e^{-j2\pi\tilde{\beta}\varepsilon T}e^{-j2\pi(\tilde{f}+\Delta f_c)(-NT)}\sum_{l=0}^{L-1}e^{-j2\pi\tilde{\beta}lT} \\
\times H(\tilde{\beta}-\tilde{f}-\Delta f_c)G(\tilde{\beta}-\tilde{f}-\Delta f_c)H^*(-\tilde{f}-\Delta f_c)G^*(-\tilde{f}-\Delta f_c), \\
\text{for CF } \tilde{\beta}=\frac{b}{(N+L)T}, b\neq k(N+L), k,b \text{ integers.}
\end{cases}
\end{aligned}
\tag{3.25}
$$

Finally, by grouping terms in (3.25), using that $\sum_{l=0}^{L-1}e^{-j2\pi\tilde{\beta}lT}$ equals L when $\tilde{\beta}=\frac{k}{T}$, while it equals $\frac{\sin(\pi\tilde{\beta}TL)}{\sin(\pi\tilde{\beta}T)}e^{-j\pi\tilde{\beta}(L-1)T}$ when $\tilde{\beta}=\frac{b}{(N+L)T}$, $b\neq k(N+L)$, one can write the SCD expression as

$$\tilde{C}_{r_{\text{CP-SCLD}}}(\tilde{\beta};\tilde{f})_{2,1} = \begin{cases} a^2 c_{s,2,1} \frac{1}{T} e^{-j2\pi\tilde{\beta}\varepsilon T}[1+\frac{2L}{N+L}\cos(2\pi(\tilde{f}+\Delta f_c)NT)] \\ \times H(\tilde{\beta}-\tilde{f}-\Delta f_c)G(\tilde{\beta}-\tilde{f}-\Delta f_c)H^*(-\tilde{f}-\Delta f_c)G^*(-\tilde{f}-\Delta f_c), \\ \text{for CF } \tilde{\beta}=\frac{k}{T}, k \text{ integer}, \\ 2a^2 c_{s,2,1}\frac{1}{(N+L)T} e^{-j2\pi\tilde{\beta}\varepsilon T}\cos(2\pi(\tilde{f}+\Delta f_c)NT)\frac{\sin(\pi\tilde{\beta}TL)}{\sin(\pi\tilde{\beta}T)}e^{-j\pi\tilde{\beta}(L-1)T} \\ \times H(\tilde{\beta}-\tilde{f}-\Delta f_c)G(\tilde{\beta}-\tilde{f}-\Delta f_c)H^*(-\tilde{f}-\Delta f_c)G^*(-\tilde{f}-\Delta f_c), \\ \text{for CF } \tilde{\beta}=\frac{b}{(N+L)T}, b\neq k(N+L), k,b \text{ integers.} \end{cases} \quad (3.26)$$

According to results in [26], $\tilde{C}_{r_{\text{SCLD}}}(\tilde{\beta};\tilde{f})_{2,1} = a^2 c_{s,2,1}\frac{1}{T}e^{-j2\pi\tilde{\beta}\varepsilon T}H(\tilde{\beta}-\tilde{f}-\Delta f_c)G(\tilde{\beta}-\tilde{f}-\Delta f_c)H^*(-\tilde{f}-\Delta f_c)G^*(-\tilde{f}-\Delta f_c)$, for $\tilde{\beta}=\frac{k}{T}$, k integer. This can be actually obtained from (3.26), for $L=0$ (no CP). Moreover, for additive white Gaussian noise (AWGN) channel $\tilde{C}^{\text{AWGN}}_{r_{\text{CP-SCLD}}}(\tilde{\beta};\tilde{f})_{2,1}$ can be simply obtained from (3.26) without considering the channel effect, i.e.,

$$\tilde{C}^{\text{AWGN}}_{r_{\text{CP-SCLD}}}(\tilde{\beta};\tilde{f})_{2,1} = \begin{cases} a^2 c_{s,2,1} \frac{1}{T} e^{-j2\pi\tilde{\beta}\varepsilon T}[1+\frac{2L}{N+L}\cos(2\pi(\tilde{f}+\Delta f_c)NT)] \\ \times G(\tilde{\beta}-\tilde{f}-\Delta f_c)G^*(-\tilde{f}-\Delta f_c), \\ \text{for CF } \tilde{\beta}=\frac{k}{T}, k \text{ integer}, \\ 2a^2 c_{s,2,1}\frac{1}{(N+L)T} e^{-j2\pi\tilde{\beta}\varepsilon T}\cos(2\pi(\tilde{f}+\Delta f_c)NT)\frac{\sin(\pi\tilde{\beta}TL)}{\sin(\pi\tilde{\beta}T)}e^{-j\pi\tilde{\beta}(L-1)T} \\ \times G(\tilde{\beta}-\tilde{f}-\Delta f_c)G^*(-\tilde{f}-\Delta f_c), \\ \text{for CF } \tilde{\beta}=\frac{b}{(N+L)T}, b\neq k(N+L), k,b \text{ integers.} \end{cases} \quad (3.27)$$

The expression for the CAF and CFs of the continuous-time signal affected by AWGN only can be also obtained from (3.19) as

$$
\tilde{c}^{\text{AWGN}}_{r_{\text{CP-SCLD}}}(\tilde{\beta};\tilde{\tau})_{2,1} =
\begin{cases}
a^2 e^{-j2\pi\Delta f_c\tilde{\tau}} c_{s,2,1} \frac{1}{T} e^{-j2\pi\tilde{\beta}\varepsilon T} \int\limits_{-\infty}^{\infty} g(t) g^*(t+\tilde{\tau}) e^{-j2\pi\tilde{\beta}t} dt, \\
\text{for delays around } \tilde{\tau} = 0\,^2, \text{ and } \tilde{\beta} = \frac{k}{T}, k \text{ integer}, \\
a^2 e^{-j2\pi\Delta f_c\tilde{\tau}} c_{s,2,1} \frac{1}{(N+L)T} e^{-j2\pi\tilde{\beta}\varepsilon T} \int\limits_{-\infty}^{\infty} \sum\limits_{l=0}^{L-1} g(t-lT) \\
\times g^*(t-lT \mp NT + \tilde{\tau}) e^{-j2\pi\tilde{\beta}t} dt, \\
\text{for delays around } \tilde{\tau} = \pm NT\,^2, \text{and } \tilde{\beta} = \frac{b}{(N+L)T}, b \text{ integer}.
\end{cases}
\tag{3.28}
$$

Similarly, expressions for the CAF, SCD, and CFs of the discrete-time signal affected by AWGN can be written based on the above results and equations (3.9) and (3.11).

3.2.2 A Necessary and Sufficient Condition on the Oversampling Factor to Eliminate Aliasing in the Cycle and Spectral Frequency Domains for CP-SCLD Signals

The SCD of a discrete-time signal is the periodic extension of the SCD of the original continuous-time signal in both spectral and cycle frequency domains [24]. This periodic extension of SCD of the original continuous-time signal leads to two kinds of aliasing, i.e., spectral and cycle aliasing [24]. Both spectral and cycle aliasing have to be eliminated when sampling is carried out. Theoretical results for the minimum sampling frequency needed to avoid aliasing is of practical interest. Here we derive a necessary and sufficient condition on the oversampling factor, ρ, to eliminate both forms of aliasing for a time dispersive channel without spectral nulls in the amplitude response (see, e.g., [20] for examples of such channels). To derive a condition to eliminate aliasing when sampling a

CP-SCLD signal, the cycle frequency domain, $\tilde{\beta}$, and spectral frequency domain, $\tilde{f}$, for which $\tilde{C}_{r_{\text{CP-SCLD}}}(\tilde{\beta};\tilde{f})_{2,1}$ is non-zero has to be first obtained. We start from the result obtained in (3.26), by considering the two branches, as follows. Based on the first branch (CFs $\tilde{\beta} = \frac{k}{T}$, k integer), the condition $|\tilde{C}_{r_{\text{CP-SCLD}}}(\tilde{\beta};\tilde{f})_{2,1}| \neq 0$ can be easily expressed as

$$|\tilde{C}_{r_{\text{CP-SCLD}}}(\tilde{\beta};\tilde{f})_{2,1}| \neq 0 \text{ if } \begin{cases} |a^2 c_{s,2,1}\frac{1}{T}e^{-j2\pi\tilde{\beta}\epsilon T}| \neq 0 & \text{(3.29a)} \\ |1+\frac{2L}{N+L}\cos(2\pi(\tilde{f}+\Delta f_c)NT)| \neq 0 & \text{(3.29b)} \\ |G(\tilde{\beta}-\tilde{f}-\Delta f_c)| \neq 0 & \text{(3.29c)} \\ |G^*(-\tilde{f}-\Delta f_c)| \neq 0 & \text{(3.29d)} \\ |H(\tilde{\beta}-\tilde{f}-\Delta f_c)| \neq 0 & \text{(3.29e)} \\ |H^*(-\tilde{f}-\Delta f_c)| \neq 0. & \text{(3.29f)} \end{cases}$$

As one can notice, conditions (3.29a)-(3.29d) represent $|\tilde{C}^{\text{AWGN}}_{r_{\text{CP-SCLD}}}(\tilde{\beta};\tilde{f})_{2,1}| \neq 0$, while conditions (3.29e)-(3.29f) are related to the channel. We first investigate the conditions to eliminate aliasing for AWGN channel and then consider the channel effect.

Condition (3.29a) is always true. (3.29b) is true if $\cos(2\pi(\tilde{f}+\Delta f_c)NT) \neq -\frac{N+L}{2L}$. Since $N > L$, then $N+L > 2L$, which yields that (3.29b) is also true. We consider that $g(t)$ is band-limited to W, with $W = \frac{1+r}{2T}$, and r is the roll-off factor (this is valid in our case, in which we use a root-rased cosine transmit filter and a low-pass receive filter to remove out-of-band noise). Based on the conditions (3.29c) and (3.29d), and by taking into account that $G(\tilde{f}) = G^*(-\tilde{f})$ one can easily show that

$$-W+\Delta f_c < \tilde{\beta}-\tilde{f} < W+\Delta f_c \tag{3.30}$$

and

$$-W-\Delta f_c < \tilde{f} < W-\Delta f_c. \tag{3.31}$$

By using (3.30) and (3.31), it is straightforward that $\tilde{\beta}$ takes values in the range

$$-2W < \tilde{\beta} < 2W. \tag{3.32}$$

By taking into account that $\tilde{\beta} = \frac{k}{T}$, one further obtains

$$-(1+r) < k < 1+r, \tag{3.33}$$

where $r \in (0,1]$. Thus, $k = 0, \pm 1$.

Moreover, to avoid cycle aliasing, f_s should satisfy the following condition,

$$f_s - 2W \geqslant 2W. \tag{3.34}$$

By replacing $f_s = \frac{\rho}{T}$, one can obtain the necessary and sufficient condition on the oversampling factor to eliminate cycle aliasing as

$$\rho \geqslant 2(1+r). \tag{3.35}$$

To avoid aliasing in the spectral frequency domain, f_s should satisfy the Nyquist condition,

$$f_s - W \geqslant W, \tag{3.36}$$

which leads to an oversampling factor

$$\rho \geqslant 1+r. \tag{3.37}$$

As such, if f_s (ρ) satisfies the condition to avoid cycle aliasing, then spectral aliasing is also avoided.

Based on the second branch of equation (3.26) (CF $\tilde{\beta} = \frac{b}{(N+L)T}$, $b \neq k(N+L)$, b, k

integers), the range of $\tilde{\beta}$ and $\tilde{f}$ values for which $|\tilde{C}_{r_{\text{CP-SCLD}}}(\tilde{\beta};\tilde{f})_{2,1}| \neq 0$ can be expressed as

$$|\tilde{C}_{r_{\text{CP-SCLD}}}(\tilde{\beta};\tilde{f})_{2,1}| \neq 0 \text{ if } \begin{cases} |2a^2 c_{s,2,1} \dfrac{1}{(N+L)T} e^{-j2\pi\tilde{\beta}\varepsilon T} e^{-j\pi\tilde{\beta}(L-1)T}| \neq 0 & (3.38a) \\ |\cos(2\pi(\tilde{f}+\Delta f_c)NT)| \neq 0 & (3.38b) \\ |\dfrac{\sin(\pi\tilde{\beta}TL)}{\sin(\pi\tilde{\beta}T)}| \neq 0 & (3.38c) \\ |G(\tilde{\beta}-\tilde{f}-\Delta f_c)| \neq 0 & (3.38d) \\ |G^*(-\tilde{f}-\Delta f_c)| \neq 0 & (3.38e) \\ |H(\tilde{\beta}-\tilde{f}-\Delta f_c)| \neq 0 & (3.38f) \\ |H^*(-\tilde{f}-\Delta f_c)| \neq 0. & (3.38g) \end{cases}$$

As for the first branch, we are first seeking the conditions to avoid aliasing for $\tilde{C}^{\text{AWGN}}_{r_{\text{CP-SCLD}}}(\tilde{\beta};\tilde{f})_{2,1}$ (equations (3.38a)-(3.38e)), and then we consider the channel effect (equations (3.38f)-(3.38g)).

One can easily notice that the condition (3.38a) is always true. Further, the condition (3.38b) is true when $2\pi(\tilde{f}+\Delta f_c)NT \neq \frac{l_1\pi}{2}$, l_1 odd integer, and the condition (3.38c) is true when $\pi\tilde{\beta}TL \neq l_2\pi$, l_2 integer ($l_2 \neq 0$, since $\tilde{\beta} \neq 0$), and $l_2 \neq l_3L$, l_3 non-zero integer ($l_2 = l_3L$ leads to $\tilde{\beta} = \frac{k}{T}$). Thus, from (3.38b) one can easily get that

$$\tilde{f} \neq \frac{l_1}{4NT} - \Delta f_c, \tag{3.39}$$

and

$$\tilde{\beta} = \frac{b}{(N+L)T} \neq \frac{l_2}{TL}, \tag{3.40}$$

(3.41)

which yields

$$b \neq \frac{l_2(N+L)}{L}, \tag{3.42}$$

where l_2 is non-zero integer, $l_2 \neq l_3 L$, l_3 integer.

Based on the conditions (3.38d) and (3.38e), and by taking into account that $G(\tilde{f}) = G^*(-\tilde{f})$, one can easily show that

$$-W + \Delta f_c < \tilde{\beta} - \tilde{f} < W + \Delta f_c \quad (3.43)$$

and

$$-W - \Delta f_c < \tilde{f} < W - \Delta f_c. \quad (3.44)$$

Furthermore, by using (3.43) and (3.44), it is straightforward that $\tilde{\beta}$ takes values in the range

$$-2W < \tilde{\beta} < 2W. \quad (3.45)$$

By taking into account that $\tilde{\beta} = \frac{b}{(N+L)T}$, $b \neq k(N+L)$, b, k integers, and $W = \frac{1+r}{2T}$, one can show that

$$-(1+r)(N+L) < b < (1+r)(N+L). \quad (3.46)$$

For example, if $r = 1$, $b \in \{-2(N+L)+1, \ldots, 2(N+L)-1\} \setminus \{0, -(N+L), (N+L)\}$.

Moreover, to avoid cycle aliasing, f_s should satisfy the condition

$$f_s - 2W \geqslant 2W. \quad (3.47)$$

By replacing $f_s = \frac{\rho}{T}$, one can then obtain the necessary and sufficient condition on the oversampling factor to eliminate cycle aliasing as

$$\rho \geqslant 2(1+r). \quad (3.48)$$

To avoid aliasing in the spectral frequency domain, f_s should satisfy the Nyquist condition

$$f_s - W \geqslant W, \quad (3.49)$$

which yields the condition on the oversampling factor to eliminate spectral aliasing as

$$\rho \geqslant 1 + r. \tag{3.50}$$

Similar to the results for CFs $\tilde{\beta} = \frac{k}{T}$, k integer (first branch), if cycle aliasing is avoided, then spectral aliasing is also avoided.

Two type of time-dispersive channels are considered in the analysis, i.e., a good channel, with no spectral nulls in the channel amplitude response, and a bad channel, with spectral nulls in the channel amplitude response [20]. When the channel amplitude response has no spectral nulls, then infinite channel bandwidth can be assumed, and the conditions (3.29e) and (3.29f) for CF $\tilde{\beta} = \frac{k}{T}$, and (3.38f) and (3.38g) for CF $\tilde{\beta} = \frac{b}{(N+L)T}$ are satisfied for any $\tilde{f}$ and $\tilde{\beta}$. On the other hand, when the channel amplitude response has spectral nulls, one can easily find the range of $\tilde{f}$ from (3.29f) and (3.38g) and show from (3.29e), (3.29f), (3.38f), and (3.38g) that $\tilde{\beta}$ belongs to a union of open intervals whose endpoints are sums of frequencies at which spectral nulls occur in the channel amplitude response. Let us denote the former by $\kappa_H^{\tilde{f}}$ and the latter by $\kappa_H^{\tilde{\beta}}$.

Following these remarks, one can conclude that if the channel is good, then the range of $\tilde{\beta}$ and $\tilde{f}$ correspond to the AWGN channel, and the conditions previously derived to avoid aliasing in both cycle and spectral frequency domains hold. If the channel is bad, then the ranges of $\tilde{\beta}$ and $\tilde{f}$ values are given by $\kappa_H^{\tilde{\beta}} \cap (-2W, 2W)$, and $\kappa_H^{\tilde{f}} \cap (-W - \Delta f_c, W - \Delta f_c)$, respectively, and corresponding values can be obtained for k, and b integers, for particular channels. If the channel bandwidth is larger than the signal bandwidth, then the domains of $\tilde{\beta}$ and $\tilde{f}$ are $(-2W, 2W)$, and $(-W - \Delta f_c, W - \Delta f_c)$ minus the endpoints in $\kappa_H^{\tilde{\beta}}$ and $\kappa_H^{\tilde{f}}$, respectively. Accordingly, the conditions on f_s (ρ) to avoid cycle and spectral aliasing are the same as in case of good channels.

3.2.3 Estimated and Theoretical CAF and SCD for CP-SCLD Signals

The estimated and theoretical CAF and SCD magnitudes of CP-SCLD signals are plotted in the absence of noise in Figs. 3.1 and 3.2, respectively. The sensing time equals 25.6 ms. A five-tap ($M = 5$) time dispersive channel is considered, with coefficients $h(\bar{\xi}_1) = 0.227$, $h(\bar{\xi}_2) = 0.46$, $h(\bar{\xi}_3) = 0.688$, $h(\bar{\xi}_4) = 0.46$, and $h(\bar{\xi}_5) = 0.688$ [27], and delays $\bar{\xi}_1, \ldots, \bar{\xi}_5$ uniformly distributed over $[0, 16\mu s]$; other parameters are set as specified in Section 4.3 of Chapter 4.

From these figures, one can easily notice that the estimated CAF and SCD magnitude of the SCLD signals are in agreement with the theoretical findings. However, a noisy floor appears due to the finite sensing time used for estimation; the shorter this time, the higher the floor.

3.3 Second-Order Cyclostationarity of SCLD and OFDM Signals

The analytical closed-form expressions for the CAF and set of CFs for the SCLD signals in (2.3) are given as (under the assumption of no aliasing) [13]

$$\begin{aligned} c_{r_{\mathrm{SCLD}}}(\beta;\tau)_{2,1} = {} & a^2 e^{-j\frac{2\pi}{\rho}\Delta f_c T \tau} c_{s,2,1} \frac{1}{\rho} e^{-j2\pi\beta\varepsilon\rho} \sum_{n=-\infty}^{\infty} \sum_{m_1=1}^{M} h(\zeta_{m_1}) g(n-\zeta_{m_1}) \\ & \times \sum_{m_2=1}^{M} h^*(\zeta_{m_2}) g^*(n+\tau-\zeta_{m_2}) e^{-j2\pi\beta n} + c_w(\beta;\tau)_{2,1}, \end{aligned} \tag{3.51}$$

and

$$\kappa_{2,1,c}^{\mathrm{SCLD}} = \left\{\beta \in [-\frac{1}{2}, \frac{1}{2} | \beta = \frac{l}{\rho}, l \text{ integer}\right\}. \tag{3.52}$$

Similar to the CP-SCLD signals, non-zero CAF is achieved only at CFs given in (3.52) and for certain delays. Results show that non-zero CAF magnitude values are obtained for delays around $\zeta_{m_2} - \zeta_{m_1}{}^2$, $m_1, m_2 = 1, \ldots, M$ [13]. Otherwise, the CAF is zero.

The analytical closed-form expressions for the CAF and the set of CFs for the OFDM signals in (2.7) are given as [13]

$$\begin{aligned} c_{r_{\text{OFDM}}}(\beta;\tau)_{2,1} = {} & a^2 c_{s,2,1} \frac{1}{D} e^{-j2\pi\beta\varepsilon D} e^{-j\frac{2\pi}{\rho K}\Delta f_c T_u \tau} \sum_{n=-\infty}^{\infty} \sum_{m_1=1}^{M} h(\zeta_{m_1}) g(n-\zeta_{m_1}) \\ & \times \sum_{m_2=1}^{M} h^*(\zeta_{m_2}) g^*(n+\tau-\zeta_{m_2}) \Xi_K(\tau,\zeta_{m_1},\zeta_{m_2}) e^{-j2\pi\beta n} \\ & + c_w(\beta;\tau)_{2,1}, \end{aligned} \tag{3.53}$$

and

$$\kappa_{2,1,c}^{\text{OFDM}} = \left\{\beta \in [-\frac{1}{2}, \frac{1}{2}) | \beta = \frac{l}{D}, l \text{ integer}\right\}, \tag{3.54}$$

where $\Xi_K(\tau,\zeta_{m_1},\zeta_{m_2}) = \sum_{k=0}^{K-1} e^{j\frac{2\pi}{\rho K}k(\tau-\zeta_{m_2}+\zeta_{m_1})}$.

Similarly, the expression for the CAF of the OFDM signals in (3.53) is valid only at CFs given in (3.54) and for certain delays. A significant non-zero value of the CAF magnitude can be noticed at delays around $\zeta_{m_2} - \zeta_{m_1}{}^2$ and $\pm\rho K + \zeta_{m_2} - \zeta_{m_1}{}^2$, $m_1, m_2 = 1, \ldots, M$, with the latter due to the existence of the CP [13].

The CAF magnitude for SCLD and OFDM signals (in time dispersive channel and in the absence of noise) is plotted versus CF and delay in Figs. 3.3 and 3.4, respectively. The sensing time and the channel are as in Section 3.2.3, and the other parameters are set as in Section 4.3 of Chapter 4. As for CP-SCLD signal, one can easily notice that simulations and theoretical results match; a noisy floor appear in the simulation results due to the finite sensing time.

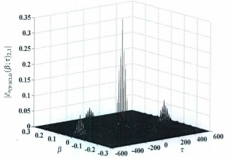

(a)

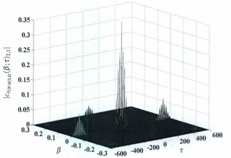

(b)

Figure 3.1: CAF magnitude of CP-SCLD signals in time dispersive channel and in the absence of noise: (a) estimated; (b) theoretical.

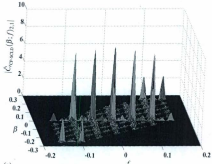

(a)

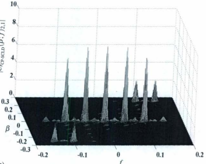

(b)

Figure 3.2: SCD magnitude of CP-SCLD signals in time dispersive channel and in the absence of noise: (a) estimated; (b) theoretical.

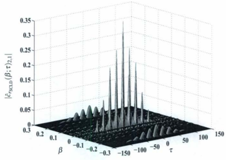

(a)

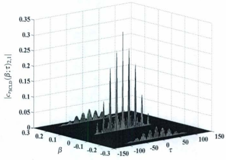

(b)

Figure 3.3: CAF magnitude of SCLD signals in time dispersive channel and in the absence of noise: (a) estimated; (b) theoretical.

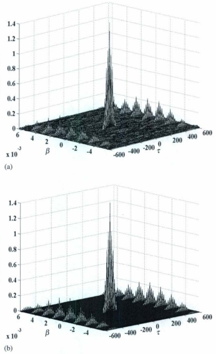

Figure 3.4: CAF magnitude of OFDM signals in time dispersive channel and in the absence of noise: (a) estimated; (b) theoretical.

3.4 Summary

In this chapter we first introduced the second-order signal cyclostationarity. The new results regarding the analytical expressions for the CAF, CF, and SCD for the CP-SCLD signal were presented. Then we discussed the findings on the condition on the oversampling factor to eliminate aliasing in both cycle and spectral frequency domains. The expressions for the CAF for SCLD and OFDM signals were provided in the end.

Chapter 4

Joint Signal Detection and Classification: Theoretical Developments, and Simulation and Experimental Performance Evaluation

In this chapter we develop a joint detection and classification algorithm for SCLD, CP-SCLD, and OFDM signals based on their second-order cyclostationarity. We first introduce the discriminating signal features, then describe the proposed algorithm, and finally, present the algorithm performance based on both simulations and experiments.

4.1 Signal Features

Based on results presented in Chapter 3, we can draw the following conclusions on the CAF magnitude of SCLD, CP-SCLD, and OFDM signals:

- The CAF of SCLD signals at zero CF is non-zero only for delays around $\zeta_{m_2} - \zeta_{m_1}$. This differs from the case of CP-SCLD and OFDM signals, for which non-zero values are also obtained for delays around $\pm\rho N + \zeta_{m_2} - \zeta_{m_1}$ and $\pm\rho K + \zeta_{m_2} - \zeta_{m_1}$ respectively, due to the existence of the CP;

- For SCLD signals, peaks in the CAF magnitude also appear at $\frac{1}{\rho}$ CF and for delays around $\zeta_{m_2} - \zeta_{m_1}$;

- The CAF and CFs of CP-SCLD signals are the same as for the SCLD signals for delays around $\zeta_{m_2} - \zeta_{m_1}$, but differ for delays around $\pm\rho N + \zeta_{m_2} - \zeta_{m_1}$, in which case the CFs are integer multiples of $\frac{1}{(N+L)\rho}$;

- For the OFDM signals, the CFs are integer multiples of $\frac{1}{D}$, with the CAF magnitude at non-zero CFs and for delays around $\zeta_{m_2} - \zeta_{m_1}$ being close to zero.

4.2 Algorithm Description

Before the signal recognition algorithm is applied, the bandwidth of the received signal is roughly estimated, the out-of-band noise removed by filtering, and the signal down-converted and oversampled. The sampling rate equals ρ times the estimated bandwidth. The baseband discrete-time signal is exploited for the identification of the signal type, as follows. First, SCLD and noise is discriminated against CP-SCLD and OFDM by using the behaviour of the CAF at zero CF over the delay range. Peaks in the CAF magnitude at non-zero delays for the CP-SCLD and OFDM signals will be exploited for their recognition against SCLD and noise. After discrimination between SCLD and noise against CP-SCLD and OFDM, recognition of CP-SCLD versus OFDM and SCLD versus noise is respectively carried out. The difference in the CAF at zero delay and over the CF range will be exploited. More specifically, the existence of peaks in the CAF magnitude at zero delay and CF equals to $\frac{1}{\rho}$ will be used to discriminate CP-SCLD against OFDM, as well as SCLD against noise.

We develop a binary decision tree algorithm with three nodes: we discriminate SCLD and noise against CP-SCLD and OFDM at Node 1, CP-SCLD and OFDM are discriminated at Node 2, while SCLD and noise are distinguished at Node 3. At each node a statistic is calculated based on the aforementioned CAF and compared against a threshold for decision making. The flowchart of the proposed algorithm is presented in Fig. 4.1.

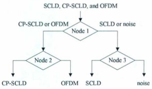

Figure 4.1: The flowchart of the proposed algorithm.

More specifically, at Node 1, the SCLD and noise are distinguished from CP-SCLD and OFDM by exploiting the existence of peaks in the CAF magnitude at zero CF and delays around $\pm\rho K + \zeta_{m_2} - \zeta_{m_1}$ for OFDM and $\pm\rho N + \zeta_{m_2} - \zeta_{m_1}$ for CP-SCLD. No such peaks exist for SCLD. The CAF magnitude of the baseband received signal is estimated at zero

CF ($\beta = 0$) and over a certain range of delay values. The range is chosen to cover possible peaks from $\min(\rho K_{\min}, \rho N_{\min})$ to $\max(\rho K_{\max}, \rho N_{\max})$, with $N_{\min}$ and $N_{\max}$ as the minimum and maximum number of information data symbols considered in a CP-SCLD signal block, respectively, and $K_{\min}$ and $K_{\max}$ as the minimum and maximum number of subcarriers that we consider for OFDM signals, respectively. The minimum delay, $\min(\rho K_{\min}, \rho N_{\min})$, must be far enough from zero to serve as an unambiguous discriminating feature. Over the considered delay range, we select the delay value for which the CAF magnitude reaches a local maximum. The cyclostationarity test developed in [28] is used to check whether or not $\beta = 0$ is indeed a CF for the selected delay. This test involves the comparison of a test statistic, calculated based on the estimated CAF at the aforementioned CF and delay, against a threshold. The threshold is chosen for a certain probability of deciding that $\beta = 0$ is a CF for the selected delay when this is actually not. Details on this test are subsequently provided. If $\beta = 0$ is found to be a CF, the signal is considered to belonging to the CP-SCLD/OFDM signal class; otherwise it is decided to belonging to SCLD/noise class.

At Node 2, CP-SCLD and OFDM signals are distinguished by using the existence of peaks in the CAF magnitude of the former at non-zero CF and zero delay. As such, the CAF magnitude of the signal is estimated at zero delay and over a range of cycle frequencies around $\frac{1}{\rho}$, excluding zero CF. The frequency for which the CAF magnitude reaches a local maximum is selected as a candidate CF. The previously mentioned cyclostationarity test is then employed to check whether or not the candidate CF is indeed a CF for zero delay. The statistic used in this test is calculated based on the estimated CAF at candidate CF and zero delay. The threshold is set for a certain probability of incorrectly deciding that the candidate CF is indeed a CF for zero delay. If the candidate CF is found to be a CF, the signal is considered to be a CP-SCLD signal; otherwise an OFDM signal.

At Node 3, discrimination between SCLD and noise is done in the same way as the discrimination between CP-SCLD and OFDM at Node 2.

Note that the proposed algorithm only relies on minimal preprocessing of the signal: after the bandwidth and the carrier frequency are estimated, the signal is filtered, down-converted and sampled. There is no requirement for the recovery of the carrier, waveform, and symbol timing information or the estimation of the noise and signal powers.

Cyclostationarity Test Used for Decision-Making with the Proposed Algorithm

A cyclostationarity test, which is developed in [28], is presented here for second-order CFs. This is used with the proposed algorithm at all three nodes for decision making. With this test, the presence of a CF is formulated as a binary hypothesis-testing problem, i.e., under hypothesis H_0 the tested frequency β is not a CF at delay τ, and under hypothesis H_1 the tested frequency β is a CF at delay τ. The cyclostationarity test consists of the following three steps:

Step 1: The CAF of the received signal $r_i(n)$ is estimated (from N_s samples) at tested frequency β and delay τ, and a vector $\hat{c}_{2,1}$ is formed as

$$\hat{c}_{2,1} = [\mathrm{Re}\{\hat{c}_{r_i}(\beta;\tau)_{2,1}\}\ \mathrm{Im}\{\hat{c}_{r_i}(\beta;\tau)_{2,1}\}], \tag{4.1}$$

where $\mathrm{Re}\{\cdot\}$ and $\mathrm{Im}\{\cdot\}$ are the real and imaginary parts, respectively.

Step 2: A statistic $\Psi_{2,1}$ is computed for the tested frequency β and delay τ,

$$\Psi_{2,1} = N_s \hat{c}_{2,1} \hat{\sum}_{2,1}^{-1} \hat{c}_{2,1}^{\dagger}, \tag{4.2}$$

where -1 denotes the matrix inverse and $\hat{\Sigma}_{2,1}$ is an estimate of the covariance matrix

$$\Sigma_{2,1} = \begin{bmatrix} \mathrm{Re}\{(Q_{2,0}+Q_{2,1})/2\} & \mathrm{Im}\{(Q_{2,0}-Q_{2,1})/2\} \\ \mathrm{Im}\{(Q_{2,0}+Q_{2,1})/2\} & \mathrm{Re}\{(Q_{2,1}-Q_{2,0})/2\} \end{bmatrix}, \tag{4.3}$$

with

$$Q_{2,0} = \lim_{N_s \to \infty} N_s \mathrm{Cum}[\hat{c}_{r_i}(\beta;\tau)_{2,1}, \hat{c}_{r_i}(\beta;\tau)_{2,1}], \tag{4.4}$$

and

$$Q_{2,1} = \lim_{N_s \to \infty} N_s \mathrm{Cum}[\hat{c}_{r_i}(\beta;\tau)_{2,1}, \hat{c}^*_{r_i}(\beta;\tau)_{2,1}]. \tag{4.5}$$

The covariances $Q_{2,0}$ and $Q_{2,1}$ are given respectively by [28] [1]

$$Q_{2,0} = \lim_{N_s \to \infty} N_s{}^{-1} \sum_{l=0}^{N_s-1} \sum_{\xi=-\infty}^{\infty} \mathrm{Cum}[f_{2,1}(l;\tau), f_{2,1}(l+\xi;\tau)] e^{-j2\pi 2\beta l} e^{-j2\pi\beta\xi}, \tag{4.6}$$

and

$$Q_{2,1} = \lim_{N_s \to \infty} N_s{}^{-1} \sum_{l=0}^{N_s-1} \sum_{\xi=-\infty}^{\infty} \mathrm{Cum}[f_{2,1}(l;\tau), f^*_{2,1}(l+\xi;\tau)] e^{-j2\pi(-\beta)l}, \tag{4.7}$$

where $f_{2,1}(l;\tau) = r_i(l) r_i{}^*(l+\tau)$ is the second-order (one-conjugate) lag product.

Step 3: The test statistic $\Psi_{2,1}$, calculated for the tested frequency β and delay τ, is compared against a threshold Γ. If $\Psi_{2,1} \geqslant \Gamma$, we decide that the tested frequency β is a CF at delay τ; otherwise not. The threshold Γ is set for a given (asymptotic) probability of false alarm, P_f, which is defined as the (asymptotic) probability to decide that the tested frequency β is a CF at tested delay τ, when it is actually not. This can be expressed as $P_f = \Pr\{\Psi_{2,1} \geqslant \Gamma | H_0\}$. By using that the statistics $\Psi_{2,1}$ has an asymptotic chi-square distribution with two degrees of freedom under the hypothesis H_0 [21], the threshold Γ can be found from the tables corresponding to this distribution.

[1] These equations are valid for zero-mean processes. For the covariance estimators see, e.g. [28], eq. (48).

4.3 Simulation and Experimental Results

4.3.1 Simulation Setup

SCLD, CP-SCLD, and OFDM signals were simulated with a 16-QAM constellation and bandwidth $B = 1.25$ MHz. The SCLD and CP-SCLD signals employed a root raised cosine pulse shape with a roll-off factor of 0.35 at the transmit side, while the OFDM signals used a raised cosine window with 0.025 roll-off factor. Unless otherwise indicated, $L = 32$ and $N = 128$ ($\frac{L}{N} = \frac{1}{4}$) for the CP-SCLD signals, and $T_{cp} = 25.6$ μs and $T_u = 102.4$ μs ($\frac{T_{cp}}{T_u} = \frac{1}{4}$) for the OFDM signals. When $\frac{L}{N} = \frac{1}{8}$ and $\frac{T_{cp}}{T_u} = \frac{1}{8}$, N and T_u were set at the same values as before. The OFDM signals employed 128 subcarriers. In addition, f_s was set to 5 MHz, Δf_c to 500 kHz, and θ and ε were random variables uniformly distributed over $[-\pi, \pi)$ and $[0, 1)$, respectively. AWGN, and ITU-R pedestrian and vehicular A fading channels were considered. The delay spread profile of the fading channels is specified in Table 4.1 [29]. The Jakes's model was used to generate multipath fading [30]. The maximum Doppler spreads of the pedestrian and vehicular fading channels were 9.72 Hz and 194.44 Hz, respectively. A Butterworth low-pass filter of order 13 was used as the receive filter. The out-of-band noise was removed at the receive side, and the signal-to-noise ratio (SNR) set at the output of the receive filter. The decision threshold was set to 27.631 at all three nodes of the algorithm. Unless otherwise indicated, sensing times of 6.4 ms and 12.8 ms were used. The probabilities of correct signal recognition, $P_{cr}^{(i|i)}$, $i =$ SCLD, CP-SCLD, and OFDM, were obtained from 1,000 trials.

	Pedestrian A channel		Vehicular A channel	
Tap no.	Delay (ns)	Power (dB)	Delay (ns)	Power (dB)
1	0	0	0	0
2	110	-9.7	310	-1
3	190	-19.2	710	-9
4	410	-22.8	1090	-10
5			1730	-15
6			2510	-20

Table 4.1: Tapped-delay-line implementation of ITU-R models [29].

4.3.2 Experimental Setup

Keithley vector signal generator (VSG 2920) and vector signal analyzer (VSA 2820) were used for experimental tests. SCLD, CP-SCLD, and OFDM signals generated in MATLAB were transmitted by using the VSG and captured with the VSA. VSG and VSA were connected through cable. The parameters of these signals were set as in Section 4.3.1. The VSG build-in mobile WiMAX OFDM signal was also used to test the proposed algorithm. The WiMAX signal bandwidth was set to 1.25 MHz, and the number of subcarriers to 128. Partial usage of subcarriers subchannelization scheme was used for both uplink and downlink subframes, with the time division duplex transmission mode. The frame size was set to 5 ms, T_u to 91.4 μs, the ratio of T_{cp} to T_u to 1:4, and the downlink-to-uplink-subframe ratio was set to 3:1. In addition, DRDC provided us with LTE downlink OFDM off the air signals, which were used to test the performance of the proposed algorithm. The LTE signal bandwidth was 10 MHz [7] and the sampling frequency was 50 MHz.

4.3.3 Performance of the Proposed Algorithm

The probabilities of correct recognition of OFDM, CP-SCLD, and SCLD signals are respectively plotted versus SNR in Figs. 4.2 (a), (b), and (c), based on both simulations (blue color) and experiments (magenta color). Results are shown for the three considered channels: AWGN (solid line), ITU-R pedestrian A (dashed line), and ITU-R vehicular A (dash-dot line). As one can see, the simulation and experimental results agree, regardless of the signal type and channel. According to Fig. 4.2(a), for the 12.8 ms sensing time, the performance for correctly recognizing OFDM signals is similar for all three channels. On the other hand, for the 6.4 ms sensing time, the performance is similar for both AWGN and pedestrian fading channels, but this significantly degrades for the vehicular fading channel. In the latter case, $P_{cr}^{(\mathrm{OFDM}|\mathrm{OFDM})}$ does not approach one. Consequently, a longer sensing time is needed to correctly recognize OFDM signals in the vehicular fading channel. In Figs. 4.2(b) and (c), similar behaviors are observed for the recognition of CP-SCLD and SCLD signals in the AWGN and pedestrian fading channels, respectively. This result holds regardless of the sensing time. Note that results for SCLD are slightly better, as the threshold at Node 1 is chosen such that the probability to decide SCLD and noise class approaches one. On the other hand, neither 6.4 ms nor 12.8 ms is sufficient to provide an acceptable performance in the vehicular fading channel, even with an increase in the SNR. Hence, we further investigate the effect of increasing the sensing time on the performance attained in this channel for CP-SCLD and SCLD signals. Results presented in Fig. 4.3 indicate that a longer sensing time is required to achieve a reasonable performance for CP-SCLD signals. For example, 512 ms sensing time is needed to achieve a probability of correct recognition of almost one at 0 dB SNR. Similar results are obtained for SCLD signals. Also, it should be noted that findings based on experiments match those obtained from simulations. These are not shown in Fig. 4.3, though, for the presentation clarity.

Note that the probability of correctly deciding noise only approaches one over the investigated SNR range (-10 dB to 10 dB), regardless of the channel. In addition, although results are presented here for 16-QAM, the performance obtained with other M-ary QAM and PSK signal constellations is similar.

The performance in recognizing the VSG build-in mobile WiMAX and LTE downlink off the air signals as OFDM signals are presented in Fig. 4.4. One can notice a degradation of performance for WiMAX OFDM signal recognition when compared with the simulation results of generic OFDM signals. This can be easily explained, for the build-in mobile WiMAX OFDM signal only $K = 84$ out of 128 fast Fourier transform points contain data, which leads to a lower value of the CAF magnitude at zero CF and delay corresponding to the useful symbol duration (see eq. (3.53)), and, thus, to a decrease in the recognition performance. The performance in recognizing the LTE OFDM off the air signal is reasonable; note that the channel is not known in this case.

The performance of the proposed signal recognition algorithm was also investigated for different CP durations for OFDM and CP-SCLD signals. Results are presented in Fig. 4.5(a) for OFDM signals with $\frac{T_{cp}}{T_u} = \frac{1}{8}$ and in Fig. 4.5(b) for CP-SCLD signals with $\frac{L}{N} = \frac{1}{8}$. A comparison with Fig. 4.2 shows that the reduction in the cyclic prefix duration adversely affects the performance for the same sensing times and channels. For example, the 6.4 ms sensing time does not provide an acceptable performance for the recognition of the OFDM signal in the vehicular fading channel, regardless of the SNR, and a longer sensing time is needed. This can be easily explained by the reduction in the correlation with reduced CP duration. On the other hand, neither 6.4 ms nor 12.8 ms are enough to

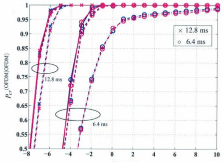
P_{cr} (OFDM|OFDM)
12.8 ms
6.4 ms
× 12.8 ms
○ 6.4 ms
SNR (dB)

(a)

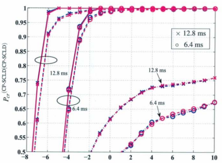
P_{cr} (CP-SCLD|CP-SCLD)
12.8 ms
6.4 ms
12.8 ms
6.4 ms
× 12.8 ms
○ 6.4 ms
SNR (dB)

(b)

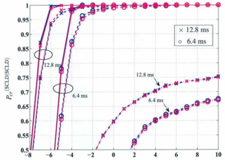

(c)

Figure 4.2: The probability of correct recognition versus SNR for (a) OFDM ($\frac{T_{cp}}{T_u} = \frac{1}{4}$), (b) CP-SCLD ($\frac{L}{N} = \frac{1}{4}$), and (c) SCLD signals, propagating through AWGN (solid line), and ITU-R pedestrian A (dashed line) and vehicular A (dash-dot line) fading channels.

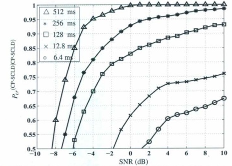

Figure 4.3: The probability of correct recognition versus SNR for CP-SCLD signals propagating through the ITU-R vehicular A fading channel, for different sensing times.

recognize CP-SCLD with a probability of almost one in vehicular channel, regardless of the SNR. Further simulations were run, and a larger sensing time is needed to achieve such a performance. For example, with 512 ms, this is attained at 5 dB SNR. Note that results for the recognition of the SCLD signals do not change, as these are not affected by the CP duration; the same holds when only noise is present.

4.4 Summary

In this chapter we proposed a joint detection and classification algorithm for SCLD, CP-SCLD, and OFDM signals. The algorithm is based on the second-order cyclostationarity of the signals. An evaluation of the algorithm performance was performed through simulations and experiments.

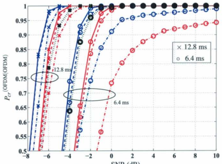

Figure 4.4: The probability of correct recognition versus SNR: simulation results for generic OFDM signals (blue color) and VSG build-in mobile WiMAX OFDM signals (red color) propagating through the channels of interested, and LTE OFDM downlink off the air signal (black color).

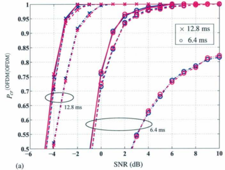

(a)

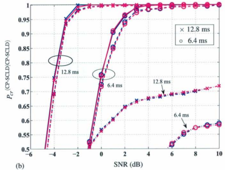

(b)

Figure 4.5: The probability of correct recognition versus SNR for (a) OFDM ($\frac{T_{cp}}{T_u} = \frac{1}{8}$) and (b) CP-SCLD ($\frac{L}{N} = \frac{1}{8}$) signals propagating through AWGN (solid line), and ITU-R pedestrian A (dashed line) and vehicular A (dash-dot line) fading channels.

Chapter 5

Blind Parameter Estimation of CP-SCLD Signals: Theoretical Developments, and Simulation and Experimental Performance Evaluation

In this chapter we develop an algorithm for blind estimation of the CP-SCLD block transmission parameters, which is based on the second-order cyclostationarity. We first introduce the cyclostationarity-based signal features that the algorithm relies on, and then present the proposed algorithm. Simulation and experimental results for the performance of the algorithm are finally provided.

5.1 Signal Features

Figs. 5.1 (a) and (b) show the CAF magnitude of CP-SCLD signal, $|c_r(0;\tau)|$, versus positive delays and $|c_r(\beta;\rho N)|$ versus β, respectively. Results are obtained with the CP-SCLD parameters set as in Section 4.3.1 of Chapter 4, in the absence of noise, and for the time dispersive channel. Based on results presented in Chapter 3, we use the following properties of the CAF magnitude of the CP-SCLD signals for parameter estimation:

- The non-zero values of the CAF magnitude at delays equal to and around $\pm\rho N+\zeta_{m_2}-\zeta_{m_1}$, which can be seen in Fig. 5.1(a). In the absence of the channel dispersion, the delays $\pm\rho N+\zeta_{m_2}-\zeta_{m_1}$ reduce to $\pm\rho N$; hence, one can conclude that there is a coarse dispersion in the CAF magnitude around the peaks corresponding to delays $\pm\rho N$, due to channel dispersion. Moreover, a fine dispersion can be noticed around each of the delays $\pm\rho N+\zeta_{m_2}-\zeta_{m_1}$ because of the signal oversampling. Note that, to represent an unambiguous signal feature, ρN must be sufficiently large, such that the corresponding CAF magnitude peak does not overlap with peaks around zero delay.

- The CFs are of the form $\frac{b}{(N+L)\rho}$, which can be seen in Fig. 5.1(b). Significant CAF magnitudes are observed for values of the integer b around zero. In addition, local peaks are seen for $b=\pm(N+L)$ (note that the latter leads to CFs of the form $\pm\frac{1}{\rho}$).

5.2 Algorithm Description

The proposed algorithm is applied after signal detection and modulation classification, which is described in Chapter 4. From previous stages, an estimate of the signal bandwidth is available, out-of-band noise removed by filtering, and the signal down-converted and

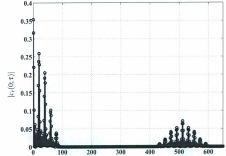

(a)

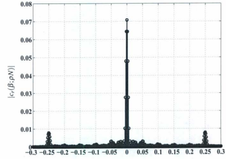

(b)

Figure 5.1: Illustration of the CP induced second-order cyclostationarity of CP-SCLD affected by a time-dispersive channel and in the absence of noise: (a) $|c_r(0;\tau)|$ versus positive delay, τ and (b) $|c_r(\beta;\rho N)|$ versus β.

oversampled at a rate equal to an integer multiple of this estimate.

The algorithm proposed for joint blind estimation of the CP-SCLD block transmission parameters consists of two steps. First, the number of data symbols in a block, N, is estimated by exploiting the existence of the CP induced peak in the CAF magnitude at delay ρN and zero CF, and then, the duration of the CP, L, is estimated based on the CP induced peaks in the CAF magnitude at delay ρN and CFs other than zero. We refer to these peaks as the CP induced peaks of interest.

At step 1, the CAF magnitude of the baseband received signal is estimated at $\beta = 0$ and over the $[\rho N_{\min}, \rho N_{\max}]$ delay range. Here $N_{\min}$ and $N_{\max}$ represent the minimum and maximum number of data symbols in a block, respectively. We choose $\rho N_{\min}$ far enough from zero, such that the peaks caused by the channel dispersion around zero delay are not considered, and $\rho N_{\max}$ large enough to cover the candidate peak. The delay value for which the CAF magnitude reaches a local maximum is selected (actually, this value is already known from the steps involved in the signal detection and classification algorithms), and the number of the data symbols in a block is chosen as the nearest integer of this delay divided by the oversampling factor. This is formulated as

$$\hat{\tau} = \underset{\tau}{\operatorname{argmax}}\{|\hat{c}_r(0;\tau)|\}, \tau \in [\rho N_{\min}, \rho N_{\max}], \tag{5.1}$$

and

$$\hat{N} = \lfloor \frac{\hat{\tau}}{\rho} \rceil, \tag{5.2}$$

where the hat symbol stands for the estimated value and $\lfloor \cdot \rceil$ denotes the nearest integer function.

At step 2, the CAF magnitude is estimated at the delay selected in Step 1, $\hat{\tau}$, and for a certain range of positive CFs. By taking into account that this range should be small to limit the number of estimates and that significant CAF magnitude values are attained only for a small number of CFs greater than zero, we limit the value of b to an adequately chosen $b_{\max}$. Moreover, as the CFs in the considered range are given by $\frac{b}{(N+L)\rho}$, with b as a positive integer and L unknown, we choose the CF range by taking into account that $0 < L < N$. The frequency for which the CAF magnitude reaches a local maximum, $\hat{\beta}$, is selected as

$$\hat{\beta} = \underset{\beta}{\operatorname{argmax}}\{|\hat{c}_r(\beta;\hat{\tau})|\}, \beta \in (\frac{1}{2\hat{N}\rho}, \frac{b_{\max}}{\hat{N}\rho}), \tag{5.3}$$

where $\hat{N}$ is obtained in Step 1. Then, the CP duration is estimated as

$$\hat{L} = \lfloor \frac{b}{\hat{\beta}\rho} - \hat{N} \rceil, \tag{5.4}$$

where b is the minimum integer between 1 and $b_{\max}$ for which a positive value is obtained for $\hat{L}$. Note that although theoretically the maximum peak is achieved for $b = 1$, another peak may be actually selected under small observation interval and low SNR conditions, which justifies the consideration of $b \in [1, b_{\max}]$. If $b_{\max}$ is too large, the peaks are too low and a search over a longer interval is performed without any contribution to the performance; we selected $b_{\max}$ such that the peaks can improve the performance at low SNR and for lower sensing time.

From the above one can notice that the proposed algorithm does not require carrier, waveform, and symbol timing recovery, and estimation of noise and signal power, which represents an important advantage.

5.3 Simulation and Experimental Results

5.3.1 Simulation and Experimental Setup

Simulation experiments are used to evaluate the performance of the estimators proposed in (5.2) and (5.4). $b_{\max}$ was set to 8. Other parameters were set as mentioned in Section 4.3.1 and Section 4.3.2 of Chapter 4. The normalized mean square error (NMSE) is employed as performance measure; the normalization is performed with respect to the second power of the true parameter value. A number of 3×10^4 trials were used.

5.3.2 Performance of the Proposed Algorithm

The performance of the estimators for the number of data symbols, N and the duration of CP, L, are respectively plotted versus SNR in Figs. 5.2 (a) and (b). The case of $L = \frac{N}{4}$ is considered. Results are shown for AWGN (solid line), ITU-R pedestrian A (dotted line), and ITU-R vehicular A (dash-dot line) channels. Interestingly, the performance of both estimators does not depend significantly on the channel type. As expected, a longer sensing time leads to an improved performance.

Note that results achieved based on experiments agree very well with simulation results. This can be noticed by comparing simulation results presented in Fig. 5.2 with experimental results showed in Fig. 5.3.

We further investigate the performance of the estimators when $L = \frac{N}{8}$, and present the results in Figs. 5.4 (a) and (b). When compared with the case where $L = \frac{N}{4}$, a degradation in the performance of both estimators is noticeable. This is due to the fact that a shorter CP duration leads to a lower value of the CP induced peak in the CAF magnitude, which can be easier missed in Step 1. For example, NMSE($\hat{N}$) reaches 10^{-6} around -4.5 dB SNR with 6.4 ms observation interval when $L = \frac{N}{4}$, whereas the same performance is achieved around 0 dB SNR when $L = \frac{N}{8}$. With a larger observation interval, a similar performance can be reached at lower SNR (e.g., with 12.8 ms, around -3 dB SNR is needed to reach NMSE($\hat{N}$) $= 10^{-6}$ when $L = \frac{N}{8}$ when compared to -6.5 dB when $L = \frac{N}{4}$).

Although here we do not show the experimental results for this case ($L = \frac{N}{8}$), we should mention that we observed a very good match with simulation results, the same as for the case $L = \frac{N}{4}$.

5.4 Summary

In this chapter we proposed an algorithm for blind parameter estimation of CP-SCLD signal. This algorithm is based on the second-order cyclostationarity of the signals. An evaluation of the algorithm performance was performed through simulations and experiments.

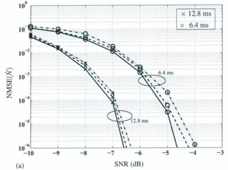

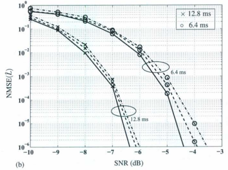

Figure 5.2: Performance for (a) $\hat{N}$ given in (5.2) and (b) $\hat{L}$ given in (5.4) (when $L = \frac{N}{4}$) versus SNR in AWGN (solid line), ITU-R pedestrian A (dotted line), and ITU-R vehicular A (dash-dot line) channels based on simulations.

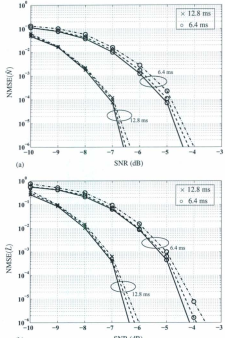

Figure 5.3: Performance for (a) $\hat{N}$ given in (5.2) and (b) $\hat{L}$ given in (5.4) (when $L = \frac{N}{4}$) versus SNR in AWGN (solid line), ITU-R pedestrian A (dotted line), and ITU-R vehicular A (dash-dot line) channels based on experimental tests.

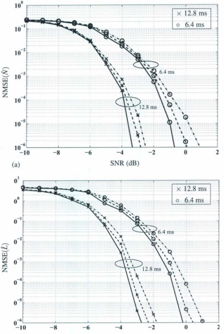

Figure 5.4: Performance for (a) $\hat{N}$ given in (5.2) and (b) $\hat{L}$ given in (5.4) (when $L = \frac{N}{8}$) versus SNR in AWGN (solid line), ITU-R pedestrian A (dotted line), and ITU-R vehicular A (dash-dot line) channels based on simulations.

Chapter 6

Conclusions and Future Work

In this thesis, the CP-SCLD signal was mathematically modeled first. Then the CP-SCLD second-order signal cyclostationarity was studied. The analytical expressions for the CAF, set of CFs, and SCD of the CP-SCLD signals were derived, as well as the condition on the oversampling factor to eliminate aliasing in both cycle and spectral frequency domains. These findings were used to select discriminating signal features and develop an algorithm for the detection and classification of CP-SCLD, OFDM, and SCLD signals. The same results were also exploited to develop an algorithm for blind parameter estimation of the CP-SCLD signals. Simulations were carried out to evaluate the performance of the proposed algorithms under diverse scenarios. Different channel conditions, sensing times, and SNRs were considered. Results showed that the proposed algorithms provide a reasonable performance under a relatively short sensing time at low SNRs, and diverse channel conditions. The proposed algorithms have the advantage of avoiding the need for carrier and symbol timing recovery, and the estimation of the signal and noise powers.

Experiments were additionally conducted to verify the theoretical findings and the simulation outcomes. These involved a Keithley vector signal generator and a Keithley vector signal analyzer. Results from experiments concurred with theoretical and simulation results, providing a strong support for the developments introduced in this thesis.

Future Work

Generic CP-SCLD signals were considered. However, in the WiMAX and LTE standards, which adopted such signals, there is supplementary information, such as preambles and pilots, which induces second-order cyclostationarity. The second-order cyclostationarity of standard CP-SCLD signals will be further exploited, and information provided by the cycle frequency domain used for signal detection, classification, and parameter estimation.

In addition, cooperative techniques will be exploited for signal detection, classification, and parameter estimation.

References

[1] *IEEE Standard for Information technology - Telecommunications and information exchange between systems - Local and metropolitan area networks - Specific requirements Part 11: Wireless LAN Medium Access Control (MAC) and Physical Layer (PHY) Specifications*, IEEE Std. 802.11, 2007.

[2] *IEEE Standard for Local and Metropolitan area networks Part 16: Air Interface for Fixed and Mobile Broadband Wireless Access Systems Amendment 2: Physical and Medium Access Control Layers for Combined Fixed and Mobile Operation in Licensed Bands and Corrigendum 1*, IEEE Std. 802.16E-2005, 2005.

[3] R. V. Nee and R. Prasad, *OFDM for Wireless Multimedia Communications*, 1st ed. Artech House, 2000.

[4] D. Falconer, S. L. Ariyavisitakul, A. Benyamin-Seeya, and B. Eidson, "Frequency domain equalization for single carrier broadband wireless systems," *IEEE Commun. Mag.*, vol. 40, pp. 58–66, Apr. 2002.

[5] H. Sari, G. Karam, and I. Jeanclaude, "Transmission techniques for digital terrestrial TV broadcasting," *IEEE Commun. Mag.*, vol. 33, pp. 100–109, Feb. 1995.

[6] B. Devillers, J. Louveaux, and L. Vandendorpe, "Exploiting cyclic prefix for performance improvement in single carrier systems," in *Proc. IEEE SPAWC*, Jul. 2006, pp. 1–5.

[7] 3GPP TS 36.211: Evolved Universal Terrestrial Radio Access (E-UTRA); Physical channels and modulation.

[8] 3GPP TS 36.101: Evolved Universal Terrestrial Radio Access (E-UTRA); User Equipment (UE) radio transmission and reception.

[9] O. A. Dobre, A. Abdi, Y. Bar-Ness, and W. Su, "A survey of automatic modulation classification techniques: classical approaches and new developments," *IET Comm.*, vol. 1, pp. 137–156, Apr. 2007.

[10] S. Haykin, "Cognitive radio: brain-empowered wireless communications," *IEEE J. Sel. Areas Commun.*, vol. 23, pp. 201–220, Feb. 2005.

[11] T. Yucek and H. Arslan, "A survey of spectrum sensing algorithms for cognitive radio applications," *IEEE Commun. Surveys Tuts.*, vol. 11, pp. 116–130, Mar. 2009.

[12] S. M. Mishra, S. ten Brink, R. Mahadevappa, and R. W. Brodersen, "Cognitive technology for ultra-wideband/wimax coexistence," in *Proc. IEEE DySPAN*, Apr. 2007, pp. 179–186.

[13] A. Punchihewa, Q. Zhang, O. A. Dobre, C. Spooner, S. Rajan, and R. Inkol, "On the cyclostationarity of ofdm and single carrier linearly digitally modulated signals in time dispersive channels: Theoretical developments and application," *IEEE Trans. Wireless Commun.*, vol. 9, pp. 2588–2599, Mar. 2010.

[14] N. Han, G. Zheng, S. H. Sohn, and J. M. Kim, "Cyclic autocorrelation based blind ofdm detection and identification for cognitive radio," in *Proc. IEEE WiCOM*, Oct. 2008, pp. 1–5.

[15] A. Bouzegzi, P. Jallon, and P. Ciblat, "A second order statistics based algorithm for blind recognition of OFDM based systems," in *Proc. IEEE GLOBECOM*, Dec. 2008, pp. 1–5.

[16] M. Oner and F. Jondral, "On the extraction of the channel allocation information in spectrum pooling systems," *IEEE J. Sel. Areas Commun.*, vol. 25, pp. 558–565, Apr. 2007.

[17] P. D. Sutton, K. E. Nolan, and L. E. Doyle, "Cyclostationary signatures in practical cognitive radio applications," *IEEE J. Sel. Areas Commun.*, vol. 26, pp. 13–24, Jan. 2008.

[18] P. D. Sutton, J. Lotze, K. E. Nolan, and L. E. Doyle, "Cyclostationary signature detection in multipath rayleigh fading environments," in *Proc. IEEE CrownCom*, Aug. 2007, pp. 408–413.

[19] F. X. Socheleau, P. Ciblat, and S. Houcke, "OFDM system identification for cognitive radio based on pilot-induced cyclostationarity," in *Proc. IEEE WCNC*, Apr. 2009, pp. 1–6.

[20] J. G. Proakis, *Digital Communications*, 4th ed. McGraw Hill, 2000.

[21] C. M. Spooner and W. A. Gardner, "The cumulant theory of cyclostationary time-series, part I: foundation and part II: development and applications," *IEEE Trans. Signal Process.*, vol. 42, pp. 3387–3429, Dec. 1994.

[22] W. A. Gardner, *Cyclostationarity in Communication and Signal Processing*. IEEE Press, 1994.

[23] A. V. Dandawate and G. B. Giannakis, "Nonparametric polyspectral estimators for kth-order (almost) cyclostationary processes," *IEEE Trans. Inf. Theory*, vol. 40, pp. 67–84, Jan. 1994.

[24] A. Napolitano, "Cyclic higher-order statistics: input/output relations for discrete- and continuous-time MIMO linear almost-periodically time-variant systems," *Signal Processing*, vol. 42, pp. 147–166, Mar. 1995.

[25] A. V. Dandawate and G. B. Giannakis, "Asymptotic theory of mixed time averages and kth-order cyclic moment and cumulant statistics," *IEEE Trans. Inf. Theory*, vol. 41, pp. 216–232, Jan. 1995.

[26] O. A. Dobre, A. Abdi, Y. Bar-Ness, and W. Su, "Cyclostationarity-based modulation classification of linear digital modulations in flat fading channels," *Wireless Personal Communications Journal*, vol. 54, pp. 699–720, Sep. 2010.

[27] S. K. Mak and A. H. Aghvami, "Detection of trellis-coded modulation on time-dispersive channels," in *Proc. IEEE GLOBECOM*, Nov. 1996, pp. 1825–1829.

[28] A. V. Dandawate and G. B. Giannakis, "Statistical test for presence of cyclostationarity," *IEEE Trans. Signal Process.*, vol. 42, pp. 2355–2369, Sep. 1994.

[29] A. F. Molisch, *Wireless Communications*, 2nd ed. Wiley, 2011.

[30] H. Harada and R. Prasad, *Simulation and Software Radio for Mobile Communications*. Artech House, 2002.